

# Gravitational waves from spinning compact binaries in hyperbolic orbits

Lorenzo De Vittori<sup>1,\*</sup>, Achamveedu Gopakumar<sup>2,†</sup>, Anuradha Gupta<sup>2</sup>, Philippe Jetzer<sup>1</sup>

<sup>1</sup>*Physik-Institut, Universität Zürich, 8057 Zürich, Switzerland*

<sup>2</sup>*Department of Astronomy and Astrophysics, Tata Institute of Fundamental Research, Mumbai 400005, India*

Compact binaries in hyperbolic orbits are plausible gravitational wave (GW) sources for the upcoming and planned GW observatories. We develop an efficient prescription to compute post-Newtonian (PN) accurate ready-to-use GW polarization states for spinning compact binaries, influenced by the dominant order spin-orbit interactions, in hyperbolic orbits. This is achieved by invoking the 1.5PN accurate quasi-Keplerian parameterization for the radial sector of the orbital dynamics. We probe the influences of spins and gravitational radiation reaction on  $h_+$  and  $h_\times$  during the hyperbolic passage. It turns out that both polarization states exhibit the memory effect for GWs from spinning compact binaries in hyperbolic orbits. In contrast, only cross polarization state exhibits the memory effect for GWs from non-spinning compact binaries. Additionally, we compute 1PN accurate amplitude corrected GW polarization states for hyperbolic non-spinning compact binaries in a fully parametric manner and perform initial comparisons with the existing waveforms.

PACS numbers: 04.30.-w, 04.80.Nn, 97.60.Lf

## I. INTRODUCTION

Compact binaries in unbound orbits are plausible GW sources for both the ground and space based GW observatories [1]. These rare events are expected to occur in dense stellar environments that are present in globular clusters and galactic nuclear clusters [2]. Interestingly, such close encounters can, in principle, create bound binaries having very high eccentricities [3, 4]. For the ground based detector like the advanced LIGO [5], the plausible detection rates for such eccentric binaries may become comparable to that for isolated compact binary coalescences, estimated to be between few to thousands per year [6]. Very recently, it was pointed out that electro-magnetic flares may accompany close encounters associated with compact binaries in hyperbolic orbits, provided such binaries contain a neutron star [7]. These electro-magnetic flashes, termed as the resonant shattering flares, arise due to the possible crustal shattering of the neutron star during its hyperbolic passage. The shattering develops because of the excitation of certain interface modes due to the extraction of orbital kinetic energy through resonant tidal coupling. This astrophysically plausible scenario should be an interesting candidate for triggered GW burst searches as it involves certain electro-magnetic flares of estimated luminosity  $\sim 10^{47}$  erg/s [7].

The investigations dealing with compact binaries in hyperbolic orbits had a chequered history and we begin by listing papers that provided inputs required to construct the associated GW polarization states. The quadrupolar order gravitational radiation field associated with two non-spinning compact objects moving in Newtonian hy-

perbolic orbits was analyzed by Turner [8]. Its extension to the first post-Newtonian (1PN) order is available in Ref. [9] while invoking the quasi-Keplerian approach to describe 1PN accurate hyperbolic orbits [10]. Note that the 1PN accurate orbital dynamics include general relativity based corrections to compact binary dynamics that are accurate to  $(v/c)^2$  order beyond the Newtonian description, where  $v$  and  $c$  are the orbital and light speeds, respectively. The explicit 1PN order amplitude corrected expressions for the two GW polarization states,  $h_+$  and  $h_\times$ , are available in Ref. [11]. This paper employed certain generalized true anomaly parameterization, detailed in Ref. [12], to describe 1PN accurate hyperbolic orbits. Additionally, there exists a number of investigations that probed various theoretical and observational aspects of non-spinning compact binaries in hyperbolic orbits. This includes quadrupolar order energy and angular momentum losses during hyperbolic encounters and its 1PN extensions [13, 14]. Aspects of gravitational bremsstrahlung involving large eccentricities and impact parameters were investigated in Ref. [15]. Recently, Ref. [16] obtained a general analytic formula for the GW energy spectrum associated with compact binaries in unbound orbits that generalized the parabolic limit computed in Ref. [17]. The quadrupolar order GW strain amplitudes and certain crude estimates for the expected rates of close gravitational flybys for terrestrial GW interferometers were reported in Ref. [18]. It was argued in Ref. [19] that GW burst signals, associated with stellar mass compact objects in nearly parabolic orbits around massive black hole (BH), should be present in a LISA-type space based GW observatory data streams. More recently, event rates for such extreme-mass-ratio bursts and the associated GW measurement accuracies for the massive BH mass and spin were explored in Refs. [20–22].

In this paper, we obtain temporally evolving GW polarization states for spinning compact binaries in PN ac-

\*lorenzo@physik.uzh.ch

†gopu@tifr.res.in

curate hyperbolic orbits. The spin effects are due to the leading order spin-orbit interactions, as detailed in Ref. [23], and the conservative non-spinning orbital dynamics is 1PN accurate. This implies that our orbital dynamics is fully 1.5PN accurate while considering compact binaries containing maximally spinning BHs. This is because the spin-orbit contributions to the orbital dynamics manifest at 1.5PN order for maximally spinning BH binaries [24]. Additionally, we incorporate the quadrupolar order gravitational radiation reaction effects while computing  $h_+(t)$  and  $h_\times(t)$ . The plots for GW polarization states having quadrupolar order amplitudes and PN accurate orbital evolution reveal that both polarization states exhibit the *memory effect* with the inclusion of spin effects. In contrast, only the plus polarization state exhibits the memory effect for non-spinning compact binaries [9, 25, 26]. Recall that Ref. [27] coined the non-vanishing difference between the wave amplitudes at  $t = \pm\infty$  as the *memory effect* while dealing with non-spinning compact binaries. This is a *linear* memory effect in contrast to the non-linear memory effect present in GW polarization states for compact binaries in bound orbits [26]. The influences of orbital eccentricity, mass ratio and initial dominant spin orientation on the observed memory effect are also probed. We observe that the memory amplitude approaches zero as orbital eccentricity tends to unity while time domain GW polarization states develop sharply varying features for low eccentricities. The GW memory amplitude is larger for the cross polarization compared to the plus polarization and weakly depends on the mass ratio. The amplitude of the memory effect slowly changes as we vary the initial orientation of the dominant spin. These changes are more visible for the plus polarization state for higher eccentricities. Additionally, we provide 1PN accurate amplitude corrected expressions for the two GW polarization states associated with hyperbolic spinning compact binaries in a fully parametric way. These expressions generalize the computations of Ref. [11] that dealt with non-spinning compact binaries in hyperbolic orbits. We observe that our approach to compute  $h_+(t)$  and  $h_\times(t)$  should be accurate and computationally cheaper than the one in [11]. This is because of invoking Mikkola's method [28] to solve the 1PN accurate Kepler Equation for hyperbolic orbits.

We provide an explanation for the presence of the linear memory effect in both the polarization states for spinning compact binaries in hyperbolic orbits. For this purpose, we follow the arguments that are used to explain the presence of this effect in certain components of the far-zone metric associated with non-spinning compact binaries in hyperbolic orbits. We show that these arguments ensure the presence of the linear memory effect in the quadrupolar order cross polarization state for non-spinning compact binaries in hyperbolic orbits. This is beneficial as we can pinpoint terms that cause the effect in the case of non-spinning compact binaries. In contrast, we argue that the memory effect arises from the combined influences of a number of terms that are present in both

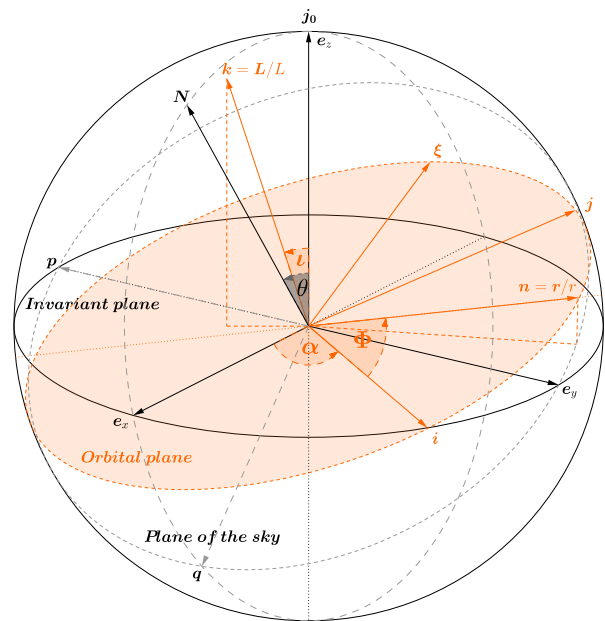


FIG. 1: Various inertial and non-inertial coordinate systems that are useful to describe the dynamics of spinning compact binaries and associated GWs. The depicted vectors  $(\mathbf{n}, \boldsymbol{\xi}, \mathbf{k})$  and  $(\mathbf{i}, \mathbf{j}, \mathbf{k})$  define the two non-inertial frames, namely the co-moving and the orbital triads. The two inertial frames associated with  $\mathbf{j}_0$  and  $\mathbf{N}$  are also displayed, namely  $(\mathbf{e}_x, \mathbf{e}_y, \mathbf{e}_z)$  and  $(\mathbf{p}, \mathbf{q}, \mathbf{N})$ . The orbital phase  $\Phi$  of the binary requires us to invoke the two vectors  $\mathbf{n}$  and  $\mathbf{i}$  while the orientation of orbital angular momentum is specified by the two angles  $\iota$  and  $\alpha$  present in the  $\mathbf{j}_0$  based inertial frame. The  $(\mathbf{p}, \mathbf{q}, \mathbf{N})$  frame is essentially specified by the angle  $\theta$  between  $\mathbf{N}$  and  $\mathbf{j}_0$ . It should be noted that the orbital plane  $(\mathbf{i}, \mathbf{j}, \mathbf{k})$  precesses around  $\mathbf{j}_0$  due to spin-orbit coupling.

polarization states associated with spinning compact binaries. Invoking non-spinning compact binaries in PN accurate orbits also allow us to compare GW polarization states from our approach with those available in the literature. Influenced by Figs. 6 to 10 in Ref. [11], we plot Newtonian, 0.5PN and 1PN contributions to  $h_+$  and  $h_\times$  for non-spinning compact binaries in hyperbolic orbits. A visual comparison reveals substantial differences the way Newtonian and 0.5PN contributions to  $h_\times$  evolve during the hyperbolic passage in our approach and the one detailed in Ref. [11]. However, the plots in Fig. 8 of Ref. [11] for their 1PN order multipolar corrections to  $h_+$  and  $h_\times$  look qualitatively similar to our plots for the 1PN order amplitude corrections to GW polarizations states. We provide a possible qualitative explanation for these differences. Our approach indeed reproduces the temporal evolution for the real and imaginary parts of the time derivatives of mass and current multipole moments and associated GW modes computed in Refs. [9, 26]. We have invoked Fig. 8 in [9] and Fig. 2 in [26] for such comparisons.

The paper is organized in the following way. In Sec. II we present our approach to obtain temporally evolving

GW polarization states for spinning compact binaries in hyperbolic orbits during their close encounters. We focus on non-spinning compact binaries in Sec. III influenced by Ref. [11] and visually compare the evolution of  $h_{\times}$  and  $h_{+}$  in these two approaches. A brief summary, possible consequences and extensions are listed in Sec. IV.

$$\begin{aligned}
h_{+|Q}(t) &= \frac{2Gm\eta}{c^4 R} \left\{ (\dot{r}^2 - z) \left[ (\sin\alpha \cos\Phi + \cos\iota \cos\alpha \sin\Phi)^2 - (C_\theta(\cos\Phi \cos\alpha - \sin\alpha \cos\iota \sin\Phi) - S_\theta \sin\iota \sin\Phi)^2 \right] \right. \\
&\quad + r^2 \dot{\Phi}^2 \left[ (\cos\alpha \cos\iota \cos\Phi - \sin\alpha \sin\Phi)^2 - (C_\theta \sin\alpha \cos\iota \cos\Phi + C_\theta \cos\alpha \sin\Phi - S_\theta \sin\iota \cos\Phi)^2 \right] \\
&\quad - r \dot{r} \dot{\Phi} \left[ \cos^2\alpha \cos\Phi \sin\Phi (\cos^2\iota + C_\theta^2) + \cos\alpha (\cos^2\Phi - \sin^2\Phi) (\cos\iota \sin\alpha (1 + C_\theta^2) + C_\theta S_\theta \sin\iota) \right. \\
&\quad \left. - \cos\Phi \sin\Phi ((1 + \cos^2\iota C_\theta^2) \sin^2\alpha + 2C_\theta S_\theta \cos\iota \sin\alpha \sin\iota + \sin^2\iota S_\theta^2) \right] \left. \right\}, \quad (2.1) \\
h_{\times|Q}(t) &= \frac{4Gm\eta}{c^4 R} \left\{ (\dot{r}^2 - z) \left[ (\sin\alpha \cos\Phi + \cos\iota \cos\alpha \sin\Phi)(C_\theta(\cos\Phi \cos\alpha - \sin\alpha \cos\iota \sin\Phi) - S_\theta \sin\iota \sin\Phi) \right] \right. \\
&\quad - r^2 \dot{\Phi}^2 \left[ (\cos\iota \cos\Phi \cos\alpha - \sin\alpha \sin\Phi)(C_\theta(\cos\Phi \sin\alpha \cos\iota + \cos\alpha \sin\Phi) + S_\theta \sin\Phi \sin\iota) \right] \\
&\quad + r \dot{r} \dot{\Phi} \left[ \cos^2\alpha \cos\iota C_\theta (\sin^2\Phi - \cos^2\Phi) + \sin\alpha (\cos^2\Phi - \sin^2\Phi) (\cos\iota C_\theta \sin\alpha + \sin\iota S_\theta) \right. \\
&\quad \left. + 2\cos\alpha \cos\Phi \sin\Phi ((1 + \cos^2\iota) C_\theta \sin\alpha + \cos\iota \sin\iota S_\theta) \right] \left. \right\}, \quad (2.2)
\end{aligned}$$

where  $R$ ,  $S_\theta$  and  $C_\theta$  stand for the radial distance to the binary,  $\sin\theta$  and  $\cos\theta$ , respectively, and  $z = Gm/r$ , where  $G$  denotes the gravitational constant. We would like to warn the reader that at few places the character  $z$  is also associated with the unit vector  $\mathbf{z}$ , the  $z$ -axis of our Cartesian coordinate system and the  $z$ -component of unit vectors like  $\mathbf{k}_z$ , as commonly used in the literature. The angle  $\theta$  provides the angle between the line of sight vector  $\mathbf{N}$  and  $\mathbf{j}_0$ , the unit vector along the direction of the total angular momentum at the initial epoch (see Fig. 1). The above expressions are provided in an inertial frame where  $\mathbf{j}_0$  points along the  $z$ -axis and where the dynamical angular variable  $\Phi$  measures the orbital phase from the line of nodes that coincides with the unit vector  $\mathbf{i}$  in a plane perpendicular to  $\mathbf{L}$ . Additionally,  $r$  and  $\dot{r}$  denote the radial orbital separation and its time derivative, respectively, while  $\dot{\Phi} = d\Phi/dt$ . The angles  $\iota$  and  $\alpha$  specify the orientation of the orbital angular momentum  $\mathbf{L}$  in the  $\mathbf{j}_0$  based inertial frame. In particular,  $\iota$  specifies the angle between the orbital angular momentum  $\mathbf{L}$  and the  $z$ -axis of the inertial frame while  $\alpha$  denotes the angle between the  $y$  axis and the projection of  $\mathbf{L}$  onto the  $x - y$  plane of the  $\mathbf{j}_0$  based inertial frame. The notations  $m$  and  $\eta$  stand for  $m = m_1 + m_2$  and  $\eta = m_1 m_2 / m^2$ . In what follows, we sketch briefly how we obtained the above expressions for  $h_{+|Q}(t)$  and  $h_{\times|Q}(t)$ .

It is customary to compute PN accurate expressions for GW polarization states from the following formulae

## II. WAVEFORMS FOR SPINNING COMPACT BINARIES IN HYPERBOLIC ORBITS

We begin by listing the explicit expressions for the quadrupolar order GW polarization states for spinning compact binaries moving in non-circular orbits.

that contain  $h_{ij}^{\text{TT}}$ , the transverse-traceless part of the radiation field:

$$h_{+} = \frac{1}{2} (p_i p_j - q_i q_j) h_{ij}^{\text{TT}}, \quad (2.3a)$$

$$h_{\times} = \frac{1}{2} (p_i q_j + p_j q_i) h_{ij}^{\text{TT}}, \quad (2.3b)$$

where the vectors  $\mathbf{p}$  and  $\mathbf{q}$  form an orthonormal triad with the line-of-sight unit vector  $\mathbf{N}$  such that  $\mathbf{p} = \mathbf{N} \times \mathbf{j}_0$  and  $\mathbf{q} = \mathbf{N} \times \mathbf{p}$  [29]. To compute the quadrupolar order GW polarization states, we require the expression for  $h_{ij}^{\text{TT}}$  that arises from the time varying Newtonian order quadrupole moment of the binary. The quadrupolar order contribution to  $h_{ij}^{\text{TT}}$  reads

$$h_{ij}^{\text{TT}}|_Q = \frac{4G\mu}{c^4 R} \mathcal{P}_{kmij}(\mathbf{N}) \left( v_{km} - \frac{Gm}{r} n_{km} \right), \quad (2.4)$$

where  $\mathcal{P}_{kmij}(\mathbf{N})$  is the transverse traceless projection operator projecting vectors onto the plane orthogonal to  $\mathbf{N}$  and  $\mu$  being the reduced mass ( $\mu = m_1 m_2 / m$ ). Additionally,  $v_{ij}$  and  $n_{ij}$  stand for  $v_i v_j$  and  $n_i n_j$ , where  $n_i$  and  $v_i$  denote the components of  $\mathbf{n} = \mathbf{r}/r$  and the velocity vector  $\mathbf{v} = d\mathbf{r}/dt$ . It should be noted that the dynamical variables appearing in eqs. (2.1) and (2.2) follow 1.5PN-accurate orbital evolution though we use Newtonian order expression for  $h_{ij}^{\text{TT}}$ . This is influenced by the restricted PN waveforms for quasi-circular inspiral where the orbital frequency and phase follow PN-accurate evolution though the expressions for  $h_{+}$  and  $h_{\times}$  arise from

the quadrupolar order  $h_{ij}^{TT}$ . This leads to the following symbolic expressions for  $h_{+|Q}(t)$  and  $h_{\times|Q}(t)$

$$h_{+} = \frac{2G\mu}{c^4 R} \left\{ (\mathbf{p}\cdot\mathbf{v})^2 - (\mathbf{q}\cdot\mathbf{v})^2 - z[(\mathbf{p}\cdot\mathbf{n})^2 - (\mathbf{q}\cdot\mathbf{n})^2] \right\}, \quad (2.5a)$$

$$h_{\times} = \frac{4G\mu}{c^4 R} \left\{ (\mathbf{p}\cdot\mathbf{v})(\mathbf{q}\cdot\mathbf{v}) - z(\mathbf{p}\cdot\mathbf{n})(\mathbf{q}\cdot\mathbf{n}) \right\}. \quad (2.5b)$$

It is convenient to evaluate the above dot products by expressing the vectors  $\mathbf{n}, \mathbf{v}, \mathbf{p}, \mathbf{q}$  and  $\mathbf{N}$  in a co-moving triad  $(\mathbf{n}, \boldsymbol{\xi} = \mathbf{k} \times \mathbf{n}, \mathbf{k})$ , where  $\mathbf{k}$  is the unit vector along  $\mathbf{L}$ . It is easy to deduce that the components of these three unit vectors in the  $\mathbf{j}_0$  based inertial frame are specified by the usual three Eulerian angles  $\Phi, \alpha$  and  $\iota$  [30]. In our convention, the inertial frame components of  $\mathbf{n}, \boldsymbol{\xi}$  and  $\mathbf{k}$  are given by

$$\mathbf{n} = (\cos \alpha \cos \Phi - \cos \iota \sin \alpha \sin \Phi) \mathbf{x} + \quad (2.6a)$$

$$(\sin \alpha \cos \Phi + \cos \iota \cos \alpha \sin \Phi) \mathbf{y} + (\sin \iota \sin \Phi) \mathbf{z},$$

$$\boldsymbol{\xi} = (-\cos \alpha \sin \Phi - \sin \alpha \cos \iota \cos \Phi) \mathbf{x} + \quad (2.6b)$$

$$(\cos \iota \cos \Phi \cos \alpha - \sin \alpha \sin \Phi) \mathbf{y} + (\sin \iota \cos \Phi) \mathbf{z},$$

$$\mathbf{k} = \sin \alpha \sin \iota \mathbf{x} - \cos \alpha \sin \iota \mathbf{y} + \cos \iota \mathbf{z}. \quad (2.6c)$$

Invoking three rotations that involve the above three Eulerian angles, it is straightforward to express the vectors that appear in Eqs. (2.5) in the  $(\mathbf{n}, \boldsymbol{\xi}, \mathbf{k})$  co-moving triad. The resulting expressions read

$$\mathbf{r} = r \mathbf{n}, \quad (2.7a)$$

$$\mathbf{v} = \dot{r} \mathbf{n} + r \left( \frac{d\Phi}{dt} + \frac{d\alpha}{dt} \cos \iota \right) \boldsymbol{\xi} + \quad (2.7b)$$

$$r \left( \frac{d\iota}{dt} \sin \Phi - \sin \iota \cos \Phi \frac{d\alpha}{dt} \right) \mathbf{k},$$

$$\mathbf{p} = (-\sin \alpha \cos \Phi - \cos \iota \cos \alpha \sin \Phi) \mathbf{n} \quad (2.7c)$$

$$+ (\sin \alpha \sin \Phi - \cos \iota \cos \alpha \cos \Phi) \boldsymbol{\xi}$$

$$+ \cos \alpha \sin \iota \mathbf{k},$$

$$\mathbf{q} = (\cos \alpha \cos \Phi \cos \theta - \cos \iota \sin \alpha \sin \Phi \cos \theta \quad (2.7d)$$

$$- \sin \iota \sin \Phi \sin \theta) \mathbf{n} - (\cos \alpha \sin \Phi \cos \theta$$

$$+ \sin \alpha \cos \iota \cos \Phi \cos \theta + \sin \iota \cos \Phi \sin \theta) \boldsymbol{\xi}$$

$$+ (\sin \alpha \sin \iota \cos \theta - \cos \iota \sin \theta) \mathbf{k},$$

$$\mathbf{N} = (\cos \alpha \cos \Phi \sin \theta - \cos \iota \sin \alpha \sin \Phi \sin \theta \quad (2.7e)$$

$$+ \sin \iota \sin \Phi \cos \theta) \mathbf{n} - (\cos \alpha \sin \Phi \sin \theta$$

$$+ \sin \alpha \cos \iota \cos \Phi \sin \theta - \sin \iota \cos \Phi \cos \theta) \boldsymbol{\xi}$$

$$+ (\sin \alpha \sin \iota \sin \theta + \cos \iota \cos \theta) \mathbf{k}.$$

To obtain the above expressions, we invoked the definitions for  $\mathbf{p}, \mathbf{q}$  and let  $\mathbf{j}_0, \mathbf{N}$  have the following components in the inertial frame:  $\mathbf{j}_0 = (0, 0, 1)$  and  $\mathbf{N} = (\sin \theta, 0, \cos \theta)$ . It is not difficult to verify that an explicit evaluation of Eqs. (2.5) for  $h_{+|Q}(t)$  and  $h_{\times|Q}(t)$  while employing the above expressions for  $\mathbf{n}, \mathbf{v}, \mathbf{p}, \mathbf{q}$  and  $\mathbf{N}$  results in Eqs. (2.1) and (2.2).

We obtain temporally evolving  $h_{+|Q}(t)$  and  $h_{\times|Q}(t)$  for spinning compact binaries in hyperbolic orbits by specifying how  $r, \dot{r}, \iota, \alpha, \Phi$  and  $\dot{\Phi}$  evolve in time along PN accurate hyperbolic orbits. The radial part of the dynamics is tackled in a parametric manner invoking  $v$ , a real variable along the orbit, the time eccentricity  $e_t$  and the mean motion  $\bar{n}$  associated with PN accurate hyperbolic orbits of Ref. [10]. The 1.5PN accurate parametric expressions for  $r$  and  $\dot{r}$ , adapted from Ref. [31], read

$$r = \frac{Gm}{c^2} \frac{1}{\bar{\xi}^{2/3}} \left\{ e_t \cosh v - 1 - \quad (2.8a)$$

$$\bar{\xi}^{2/3} \frac{e_t \cosh v (6 - 7\eta) + 18 - 2\eta}{6} + \bar{\xi} \frac{\Sigma}{\sqrt{e_t^2 - 1}} \right\},$$

$$\dot{r} = \bar{\xi}^{-1/3} \frac{c e_t \sinh v}{e_t \cosh v - 1} \left\{ 1 - \bar{\xi}^{2/3} \frac{6 - 7\eta}{6} \right\}, \quad (2.8b)$$

where  $\bar{\xi} = Gm\bar{n}/c^3$  and  $\Sigma$  terms are due to the spin-orbit interactions. The expression for  $\Sigma$  is defined as

$$\Sigma = \delta_1 \chi_1 q (\mathbf{k} \cdot \mathbf{s}_1) + \frac{\delta_2 \chi_2}{q} (\mathbf{k} \cdot \mathbf{s}_2), \quad (2.9)$$

where  $\delta_1 = \eta/2 + 3/4(1 - \sqrt{1 - 4\eta})$ , and  $\delta_2 = \eta/2 + 3/4(1 + \sqrt{1 - 4\eta})$  while  $q = m_1/m_2$  with  $m_1 \geq m_2$ . The dot products define the misalignments between  $\mathbf{L}$  and the two spins  $\mathbf{S}_1$  and  $\mathbf{S}_2$  while  $\chi_{1,2}$  stand for the two Kerr parameters such that  $\mathbf{S}_1 = Gm_1^2 \chi_1 \mathbf{s}_1/c$  and  $\mathbf{S}_2 = Gm_2^2 \chi_2 \mathbf{s}_2/c$ . The temporal evolution for  $r$  and  $\dot{r}$  are obtained by solving the following hyperbolic version of the classical Kepler Equation

$$\bar{n} (t - t_0) = e_t \sinh v - v, \quad (2.10)$$

where  $t_0$  is certain initial epoch. In the present investigation, we invoke an accurate and efficient numerical procedure, namely Mikkola's approach [28], to obtain  $v(t)$  from the above transcendental equation.

Let us note that the above three equations, namely Eqs. (2.8a), (2.8b) and (2.10), are adapted from Ref. [31] that obtained Keplerian type parametric solution to the radial sector of spinning compact binary dynamics in eccentric orbits. We begin by listing relevant equations that describe the above mentioned 1.5PN accurate Keplerian type parametric solution:

$$r = a_r (1 - e_r \cos u), \quad (2.11a)$$

$$l = n (t - t_0) = u - e_t \sin u, \quad (2.11b)$$

where  $u$  and  $l$  stand for the eccentric and mean anomalies. In what follows, we employ  $l$  to explore various aspects of our time domain GW polarization states as  $l$  essentially represents the scaled coordinate time. The orbital parameters  $a_r$  and  $n$  are the PN extensions of the semi-major axis and the mean motion associated with the Keplerian parametric solution to the Newtonian orbital dynamics. Additionally, the radial part of the PN accurate Keplerian type parameterization involves two

eccentricities, namely  $e_r$  and  $e_t$  [10]. These orbital elements are explicit functions of the reduced orbital energy  $E$ , reduced angular momentum  $L$ , the symmetric mass ratio  $\eta$ , the two Kerr parameters and the spin-orbit misalignments. To 1.5PN order, these parameters are given by

$$a_r = \frac{Gm}{-2E} \left\{ 1 - \frac{2E}{4c^2}(\eta - 7) - \frac{2E}{c^3} \frac{Gm \Sigma}{L} \right\}, \quad (2.12a)$$

$$e_t^2 = 1 + \frac{2EL^2}{G^2m^2} - \frac{2E}{c^2} \left( 2\eta - 2 + \frac{2EL^2}{G^2m^2} \frac{7\eta - 17}{4} \right) + \frac{4E}{c^3} \frac{Gm \Sigma}{L}, \quad (2.12b)$$

$$e_r^2 = 1 + \frac{2EL^2}{G^2m^2} - \frac{2E}{c^2} \left( 6 - \eta + \frac{2EL^2}{G^2m^2} \frac{15 - 5\eta}{4} \right) + \frac{8E}{c^3} \frac{Gm \Sigma}{L} \left( 1 + \frac{EL^2}{G^2m^2} \right), \quad (2.12c)$$

$$\xi = \left( \frac{-2E}{c^2} \right)^{3/2} \left\{ 1 - \frac{2E}{c^2}(\eta - 15) \frac{1}{8} \right\}, \quad (2.12d)$$

where  $\xi$  stands for  $Gmn/c^3$ . The structure of the two eccentricities indicate that it should be possible to express  $e_r$  in terms of  $e_t$  as a PN series employing  $\xi$  and the spin parameters (this holds true for  $a_r$ ). The resulting expressions for  $e_r$  and  $a_r$  read

$$e_r = e_t \left\{ 1 + \xi^{2/3} \frac{8 - 3\eta}{2} - \xi \frac{\Sigma}{\sqrt{1 - e_t^2}} \right\}, \quad (2.13a)$$

$$a_r = \frac{Gm}{c^2} \frac{1}{\xi^{2/3}} \left\{ 1 - \xi^{2/3} \frac{9 - \eta}{3} + \xi \frac{\Sigma}{\sqrt{1 - e_t^2}} \right\}. \quad (2.13b)$$

The 1.5PN accurate expressions for  $r$  and  $\dot{r}$  in terms of  $\bar{n}$ ,  $e_t$  and  $v$  are obtained with the help of the following steps. First, we obtain explicit 1.5PN accurate expression for  $r = a_r(1 - e_r \cos u)$  in terms of  $n$ ,  $e_t$  and  $u$  with the help of Eqs. (2.13). This leads to

$$r = \frac{Gm}{c^2} \frac{1}{\xi^{2/3}} \left\{ 1 - e_t \cos u - \frac{\xi^{2/3}}{6} \left( 18 - 2\eta + (6 - 7\eta) e_t \cos u \right) + \xi \frac{\Sigma}{\sqrt{1 - e_t^2}} \right\}. \quad (2.14)$$

To obtain its hyperbolic counterpart, we let  $u = \iota v$  and  $n = -\iota \bar{n}$ , where  $\iota = \sqrt{-1}$ , by invoking the arguments in Ref. [10]. This analytic continuation in  $E$  from  $E < 0$  to  $E > 0$  essentially works as all orbital parameters that are analytic near  $E = 0$ . We employ similar arguments to obtain  $\dot{r}(v, \bar{n}, e_t)$ , given by Eq. (2.8b), from its eccentric version computed in terms of  $u, n$  and  $e_t$ .

With the help of the above arguments and Ref. [31], we extract the following 1.5PN accurate  $\dot{\Phi}$  expression for

spinning compact binaries in hyperbolic orbits

$$\dot{\Phi} = \frac{\bar{n} \sqrt{e_t^2 - 1}}{(e_t \cosh v - 1)^2} \left\{ 1 + \xi^{2/3} \left( \frac{4 - \eta}{e_t \cosh v - 1} + \frac{\eta - 1}{e_t^2 - 1} \right) - \bar{\xi} \frac{\Sigma}{\sqrt{e_t^2 - 1}} \left( \frac{1}{e_t \cosh v - 1} + \frac{1}{e_t^2 - 1} \right) \right\} - \cos \iota \dot{\alpha}, \quad (2.15)$$

where the differential equation for  $\alpha$  arises from the precessional equation for  $\mathbf{k}$ . The above differential equation for  $\Phi$  is also adapted from its eccentric counterpart, given by Eq. (B2) in Ref. [31]. To derive Eq. (B2) in [31], one starts from the expression for  $\mathbf{v}$  in the co-moving triad  $(\mathbf{n}, \boldsymbol{\xi}, \mathbf{k})$  as given by Eq. (2.7b). This leads to the following 1.5PN accurate expression for  $\mathbf{v} \cdot \mathbf{v}$ , namely

$$v^2 = \dot{r}^2 + r^2(\dot{\Phi}^2 + 2\dot{\Phi}\dot{\alpha} \cos \iota), \quad (2.16)$$

where we have neglected the  $\mathcal{O}(1/c^6)$  order  $\dot{\alpha}^2$ ,  $i^2$  and  $\dot{\alpha}i$  terms. The next step is based on the fact that the square of the orbital velocity, extractable from the fully 1.5PN order Hamiltonian or orbital energy, does not contain any spin dependent terms. This is attributable to the employed gauge and the spin supplementary condition in Ref. [31]. This is why one obtains Newtonian order relation, namely  $v^2 = 2E + 2Gm/r$ , while computing  $v^2$  from a Hamiltonian that only contains Newtonian and 1.5PN order spin-orbit contributions. This statement may be verified by inspecting the Eqs. (1), (5), (10) and (39) of [31]. Therefore, the  $v^2$  expression that arise from a fully 1.5PN accurate orbital energy for spinning binaries in general orbits will not explicitly contain any spin-orbit contributions similar to the parametric equation for  $\dot{r}$ , given by Eq. (2.8b). The PN-accurate expression for  $v^2$  is given by

$$v^2 = 2E + 2 \frac{Gm}{r} + \frac{1}{c^2} \left\{ (9\eta - 3) E^2 + \frac{Gm}{r} (14\eta - 12) E + \frac{G^2m^2}{r^2} (5\eta - 10) + \frac{Gm\eta}{r^3} L^2 \right\}, \quad (2.17)$$

The expression for  $\dot{\Phi}^2$  follows by equating the above two expressions for  $v^2$ . This leads to PN accurate expression for  $\dot{\Phi}$ , as given by Eq. (B2) in [31], where the spin-orbit contributions arise from the PN accurate expression for  $r$ . We obtain our Eq. (2.15) for  $\dot{\Phi}$  with the help of earlier mentioned analytic continuation after expressing  $(-2E)$  and  $L$  in terms of  $n, e_t$  and  $u$ . For easy visualization, it is convenient to characterize our hyperbolic binaries in terms of an impact parameter  $b$  such that  $b\mathbf{v}_\infty = |\mathbf{r} \times \mathbf{v}|$  when  $|\mathbf{r}| \rightarrow \infty$  and where  $\mathbf{v}_\infty$  stands for the relative velocity at infinity. We characterize our hyperbolic binaries using the following 1PN accurate expression for  $b$  in terms of  $\xi$  and  $e_t$

$$b = \frac{Gm}{c^2} \frac{\sqrt{e_t^2 - 1}}{\xi^{2/3}} \left\{ 1 - \xi^{2/3} \left( \frac{\eta - 1}{e_t^2 - 1} + \frac{7\eta - 6}{6} \right) \right\}. \quad (2.18)$$

The temporal evolution for  $\alpha$  and  $\iota$ , as expected, requires us to solve the precessional equation for  $\mathbf{k}$  in the  $\mathbf{j}_0$  based inertial frame and this is clearly due to the Eq. (2.6c) for  $\mathbf{k}$ . In practice, we numerically solve coupled precessional equations for  $\mathbf{s}_1, \mathbf{s}_2$  and  $\mathbf{k}$  as the differential equation for  $\mathbf{k}$  arises from the relation  $\dot{\mathbf{k}} = -(S_1 \dot{\mathbf{s}}_1 + S_2 \dot{\mathbf{s}}_2)/L$ . This equation, as expected, arises from the conservation of the total angular momentum and the magnitude of the orbital angular momentum during the precessional timescale. The relevant equations that incorporate the dominant order spin-orbit coupling for binaries in hyperbolic orbits are given by

$$\dot{\mathbf{s}}_1 = \frac{c^3}{Gm} \frac{\bar{\xi}^{5/3} \sqrt{e_t^2 - 1}}{(e_t \cosh v - 1)^3} \delta_1 \mathbf{k} \times \mathbf{s}_1, \quad (2.19a)$$

$$\dot{\mathbf{s}}_2 = \frac{c^3}{Gm} \frac{\bar{\xi}^{5/3} \sqrt{e_t^2 - 1}}{(e_t \cosh v - 1)^3} \delta_2 \mathbf{k} \times \mathbf{s}_2, \quad (2.19b)$$

$$\dot{\mathbf{k}} = \frac{c^3}{Gm} \frac{\bar{\xi}^2 (\delta_1 \chi_1 q \mathbf{s}_1 + \delta_2 \chi_2 / q \mathbf{s}_2) \times \mathbf{k}}{(e_t \cosh v - 1)^3}. \quad (2.19c)$$

The expressions for  $\mathbf{s}_1$  and  $\mathbf{s}_2$  are adapted from Ref. [23] while invoking the Newtonian accurate  $L$  for hyperbolic orbits and the Newtonian version of our Eqs. (2.8) for  $r$ . Additionally, we employ the following expression for  $\dot{\alpha}$  that appear in the differential equation for  $\Phi$ . This equation arises from the Cartesian components of  $\mathbf{k}$  in the  $\mathbf{j}_0$  based inertial frame and Eq. (2.19c) for  $\dot{\mathbf{k}}$ :

$$\dot{\alpha} = \frac{k_x \dot{k}_y - k_y \dot{k}_x}{k_x^2 + k_y^2}. \quad (2.20)$$

It is possible to incorporate numerically the effects of GW emission during the hyperbolic encounter. This is achieved by solving the following 2.5PN order coupled differential equations for  $\bar{n}$  and  $e_t$ :

$$\frac{d\bar{n}}{dt} = -\frac{c^6}{G^2 m^2} \frac{\bar{\xi}^{11/3} 8 \eta}{5 \beta^7} \times \quad (2.21a)$$

$$[-49\beta^2 - 32\beta^3 + 35(e_t^2 - 1)\beta - 6\beta^4 + 9e_t^2\beta^2],$$

$$\frac{de_t}{dt} = -\frac{c^3}{Gm} \frac{\bar{\xi}^{8/3} 8 \eta (e_t^2 - 1)}{15 \beta^7 e_t} \times \quad (2.21b)$$

$$[-49\beta^2 - 17\beta^3 + 35(e_t^2 - 1)\beta - 3\beta^4 + 9e_t^2\beta^2],$$

where, for simplicity, we write  $\beta = e_t \cosh v - 1$ . The derivation of the above two differential equations is adapted from Eqs. (63) in Ref. [32] and requires 2.5PN contributions to the relative acceleration.

We are now in a position to obtain  $h_+|_Q(t)$  and  $h_\times|_Q(t)$  for spinning compact binaries moving in hyperbolic orbits influenced by GW emission. The idea is to numerically obtain the temporal evolution for  $r, \dot{r}, \Phi, \dot{\Phi}, \iota, \alpha, \bar{n}$  and  $e_t$  and impose these variations in the expression for  $h_+|_Q(t)$

and  $h_\times|_Q(t)$ , given by Eqs. (2.1) and (2.2). We begin by specifying the initial binary configuration in terms of  $m_1, m_2, \chi_1, \chi_2, \bar{n}$  and  $e_t$ . It is possible to specify the initial orientations of  $\mathbf{s}_1, \mathbf{s}_2$  and  $\mathbf{k}$  in the  $\mathbf{j}_0$  based inertial frame by freely choosing four angles  $(\theta_1^i, \theta_2^i)$  and  $(\phi_1^i, \phi_2^i)$ . These four angles provide the six Cartesian components of  $\mathbf{s}_1$  and  $\mathbf{s}_2$  at the initial epoch and, in general, these components are

$$\mathbf{s}_1 = (\sin \theta_1 \cos \phi_1, \sin \theta_1 \sin \phi_1, \cos \theta_1), \quad (2.22a)$$

$$\mathbf{s}_2 = (\sin \theta_2 \cos \phi_2, \sin \theta_2 \sin \phi_2, \cos \theta_2). \quad (2.22b)$$

The values of  $\iota$  and  $\alpha$  that specify the initial orientation of  $\mathbf{k}$  are not freely chosen. These initial estimates are obtained by noting that the initial  $x$  and  $y$  components of  $\mathbf{j}$  should be zero as we let  $\mathbf{j}$  to point along the  $z$ -axis at the initial epoch. This leads to the following expressions for  $k_x$  and  $k_y$  at  $t = 0$

$$k_x|_{t=0} = \bar{\xi}_0^{-1/3} \frac{X_1^2 \chi_1 \sin \theta_1^i \cos \phi_1^i + X_2^2 \chi_2 \sin \theta_2^i \cos \phi_2^i}{\eta \sqrt{e_t^2 - 1}}, \quad (2.23a)$$

$$k_y|_{t=0} = \bar{\xi}_0^{-1/3} \frac{X_1^2 \chi_1 \sin \theta_1^i \sin \phi_1^i + X_2^2 \chi_2 \sin \theta_2^i \sin \phi_2^i}{\eta \sqrt{e_t^2 - 1}}, \quad (2.23b)$$

where  $X_1 = m_1/m$  and  $X_2 = m_2/m$  while  $\bar{\xi}_0$  denotes the initial value for  $\bar{\xi}$ . The initial estimates for  $\iota$  and  $\alpha$  is obtained by equating the above expressions to  $\sin \alpha \sin \iota$  and  $-\cos \alpha \sin \iota$ . However, we usually extract values of  $\alpha$  and  $\iota$  during the numerical interaction with the help of the three Cartesian components of  $\mathbf{k}$ , namely  $\alpha = -\tan^{-1}(k_x/k_y)$  and  $\iota = \cos^{-1}(k_z)$ . We impose the phasing angle  $\Phi$  to vanish at periastron time, i.e.  $\Phi(0) = 0$ .

We begin the numerical implementation of  $h_+|_Q(t)$  and  $h_\times|_Q(t)$  by obtaining  $v(t)$  and this involves solving Eq. (2.10) via the Mikkola's method. The resulting  $v(t)$  is imposed on Eqs. (2.8) for  $r(v)$  and  $\dot{r}(v)$  to obtain 1.5PN accurate  $r(t)$  and  $\dot{r}(t)$  for our hyperbolic binary configuration. The next step involves numerically integrating simultaneously the above listed differential equations for  $\mathbf{s}_1, \mathbf{s}_2, \mathbf{k}, \Phi, \bar{n}$  and  $e_t$ . This is achieved by invoking twelve differential equations that include differential equations for the nine Cartesian components of  $\mathbf{s}_1, \mathbf{s}_2$  and  $\mathbf{k}$  in the  $\mathbf{j}_0$  based inertial frame. In practice, we use the mean anomaly  $l$  rather than the coordinate time  $t$  while numerically tackling these differential equations and the transcendental equation (2.10). The change of variable is performed by noting that  $dl = \bar{n} dt$ . In what follows, we display  $h_+|_Q(l)$  and  $h_\times|_Q(l)$  resulting from such an implementation and explore various features.

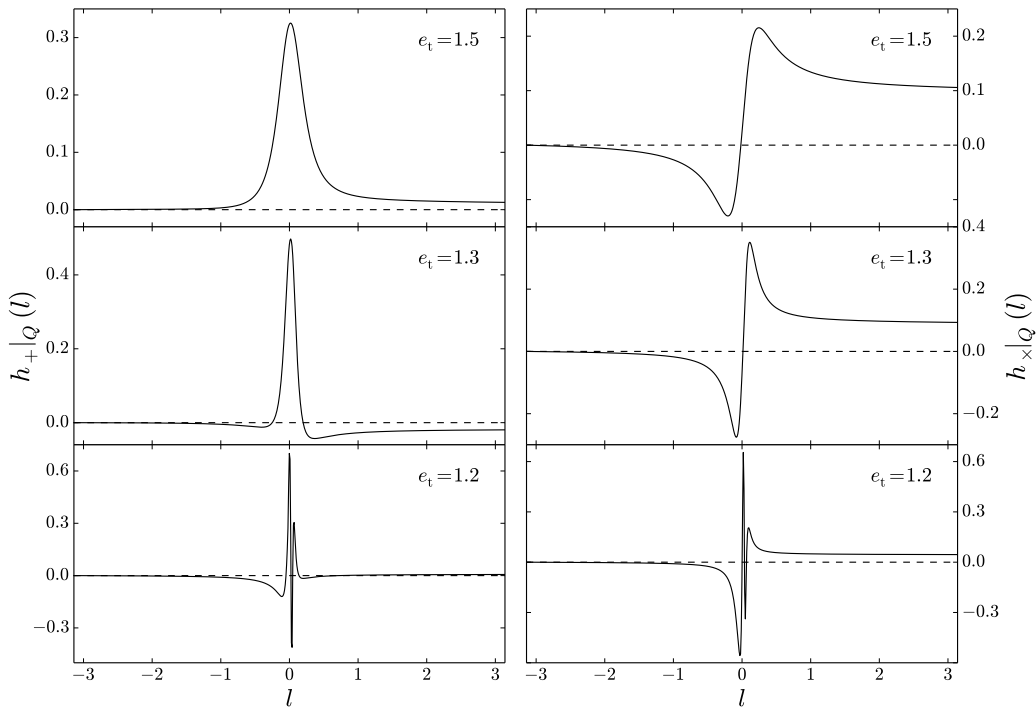


FIG. 2: The scaled  $h_{+|Q}(l)$  and  $h_{\times|Q}(l)$  plots for  $m = 20 M_{\odot}$ ,  $q = 1$  spinning compact binaries containing maximally spinning BHs. The employed scale factor in the present and the next two figures is  $Gm/c^2 R$ . We let  $e_t$  take three values while choosing  $b \sim 30 Gm/c^2$ . The initial spin orientations in the  $\mathbf{j}_0$  based inertial frame are  $\theta_1^i = 30^\circ$ ,  $\theta_2^i = 30^\circ$ ,  $\phi_1^i = 30^\circ$ ,  $\phi_2^i = 120^\circ$  and we let  $\theta = 45^\circ$ . The conservative orbital evolution is fully 1.5PN accurate and the influences of GW emission are taken into account at leading order. The linear memory effect causes the solid line waveform plots to depart from the dashed line after the hyperbolic passage.

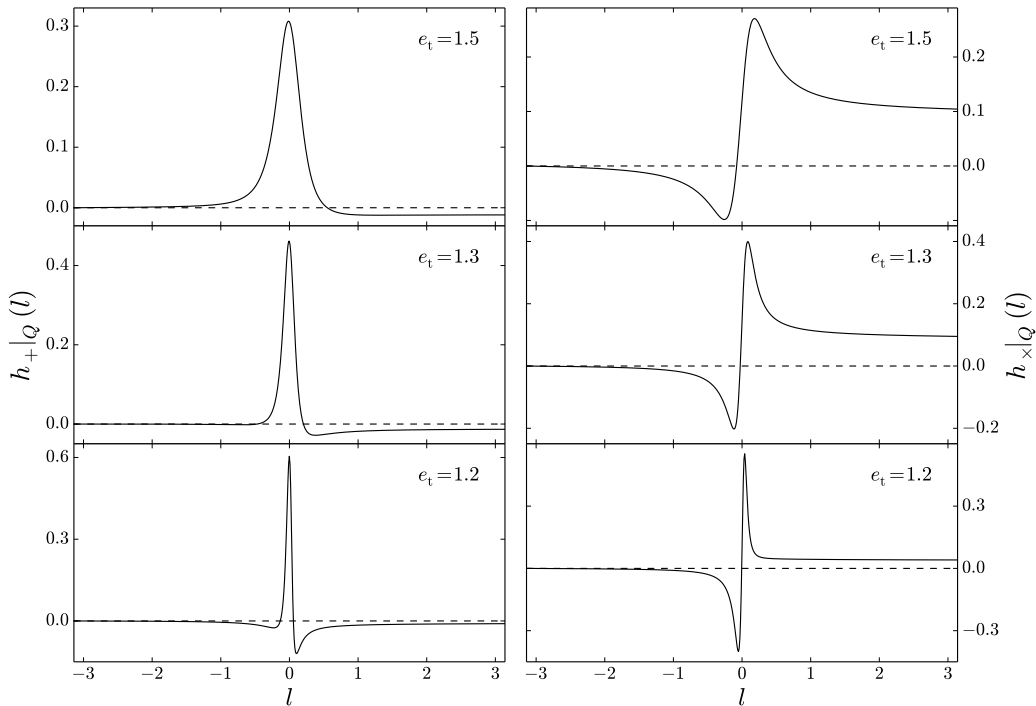


FIG. 3: The scaled  $h_{+|Q}(l)$  and  $h_{\times|Q}(l)$  plots for  $m = 20 M_{\odot}$ ,  $q = 4$  spinning compact binaries containing maximally spinning BHs. The other specifications are same as in Fig. 2. The amplitude of the memory effect is rather insensitive to the mass ratio. However, the sharply varying features with multiple peaks, present in  $e_t = 1.2$  plots of Fig. 2, are not visible.

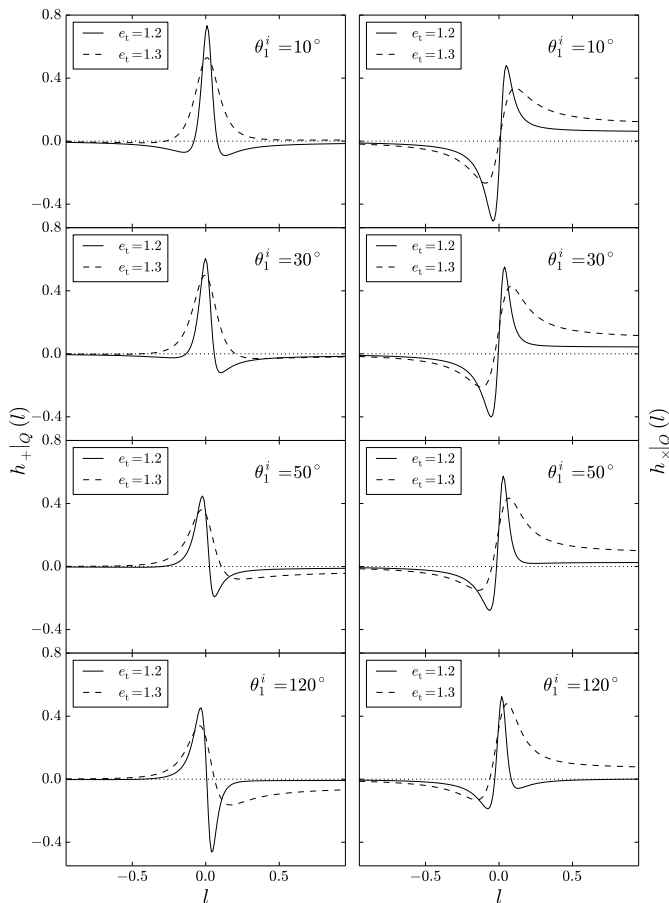


FIG. 4: We plot the scaled  $h_{+|Q}(l)$  and  $h_{\times|Q}(l)$  for  $m = 20 M_{\odot}$ ,  $q = 4$  spinning compact binaries containing maximally spinning BHs while varying the initial orientation of the dominant spin for two  $e_t$  values. The orbital dynamics is fully 1.5PN accurate while other parameters are similar to those used in Fig. 3. The impact of the initial misalignment between  $\mathbf{s}_1$  and  $\mathbf{j}_0$  on the memory is more prominent on  $h_{+|Q}(l)$  for higher  $e_t$  values.

In Figs. 2 and 3, we display  $h_{+|Q}(l)$  and  $h_{\times|Q}(l)$  for  $q = 1$  and  $q = 4$  binaries having three different orbital eccentricities. We observe that both polarization states exhibit the memory effect. It is due to this ‘linear’ memory effect that GW amplitudes at  $t = +\infty$  are different from their respective  $t = -\infty$  values, depicted by the dashed lines. The amplitude of the effect decreases as the orbital eccentricity approaches unity. However, the time-domain waveforms develop sharply varying features compared to their higher orbital eccentricity counterparts. This feature is mass ratio dependent and clearly visible for comparable mass binaries. For a given  $e_t$  and  $\bar{n}$ , the amplitude of the memory effect is larger for  $h_{\times|Q}(l)$  compared to its ‘plus’ counterpart. Note that the memory effect is absent in  $h_{+|Q}(l)$  for non-spinning binaries as evident from figures in Ref. [9, 26]. In Fig. 4, we probe the influence of the initial orientation of the dominant spin on the memory effect for  $q = 4$  unequal mass binaries. The memory amplitude decreases as we vary the initial

misalignment of  $\mathbf{s}_1$  from  $\mathbf{j}_0$  for  $e_t$  values closer to unity. The variations in the memory amplitude is more prominent for the  $h_{+|Q}(l)$  plots for higher  $e_t$  values. This may be attributed to the more pronounced orbital precession for higher  $\theta_1^i$  values and the presence of non-negligible  $\sqrt{e_t^2 - 1}$  contribution in the differential equations for the two spins, as evident from Eqs. (2.19). It will be interesting to probe any possible data analysis implications of the varying memory amplitudes as depicted in Fig. 4. We have also verified that the memory effect persists even if we switch off the effects of GW damping. In fact, the plots for  $h_{+|Q}(l)$  and  $h_{\times|Q}(l)$  are essentially identical to those displayed in Figs. 2, 3 and 4 while neglecting the effects of GW damping, provided by Eqs. (2.21).

In Appendix A, we provide formulae for computing 1PN order amplitude corrected GW polarization states for spinning binaries in a compact way. The expressions, given by Eqs. (A1), are obtained with the help of Eqs. (2.3) while using fully 1PN accurate expression for the transverse–traceless part of the radiation field  $h_{ij}^{\text{TT}}$ . The 1PN accurate expression for  $h_{ij}^{\text{TT}}$  incorporates contributions from appropriate time derivatives of various mass type and current type multipole moments of the binary and are adapted from Eqs. (3.22) in Ref. [24]. Specifically, 1PN-accurate expression for  $h_{ij}^{\text{TT}}$  requires us to compute time derivatives of mass and current quadrupoles and octopoles of the binary and fourth time derivative of  $\mathcal{I}^{ijkl}$  which is given by the symmetric and trace free part of  $\mu(1 - 3\eta) x^{ijkl}$ . We do not provide the explicit 1PN accurate amplitude contributions to  $h_{+}(l)$  and  $h_{\times}(l)$  in terms of  $\dot{r}$ ,  $z$ ,  $r \dot{\Phi}$  and trigonometric functions of  $\iota$ ,  $\alpha$  and  $\Phi$  as done in Eqs. (2.1) and (2.2). The very lengthy nature of such expressions is the main reason why we did not expand the squares and products appearing in Eqs. (A1) with the help of various dot products, given by Eqs. (A2)-(A7). It is fairly straightforward to obtain plots for the 0.5PN and 1PN contributions to  $h_{+}(l)$  and  $h_{\times}(l)$ , similar to our plots for  $h_{+|Q}(l)$  and  $h_{\times|Q}(l)$ . This is also not pursued as these PN contributions, as expected, are substantially smaller in magnitude compared to the quadrupolar order waveforms. Additionally, the plots for such PN contributions are qualitatively similar to plots for  $h_{+|Q}(l)$  and  $h_{\times|Q}(l)$  as these contributions also exhibit the linear memory effect.

In what follows, we provide an explanation for the presence of the linear memory effect in both the polarization states for spinning compact binaries in hyperbolic orbits. This explanation becomes clearer and easier while considering non-spinning compact binaries in hyperbolic orbits. In the next section, we consider temporally evolving GW polarization states associated with non-spinning compact binaries in 1PN accurate hyperbolic orbits invoking our Keplerian type parametric solution. This should also allow us to compare our 1PN accurate  $h_{+}(l)$  and  $h_{\times}(l)$  with those obtained via the generalized true anomaly parameterization, detailed in Ref. [11].



### III. 1PN ACCURATE GRAVITATIONAL WAVE PHASING FOR NON-SPINNING COMPACT BINARIES IN HYPERBOLIC ORBITS

We begin by constructing quadrupolar order GW polarization states, namely  $h_{+|Q}(l)$  and  $h_{\times|Q}(l)$ , associated with non-spinning compact binaries moving in 1PN accurate hyperbolic orbits. It is not very difficult to infer that Eqs. (2.5) that provide  $h_{+|Q}(l)$  and  $h_{\times|Q}(l)$  in terms of various dot products involving  $\mathbf{p}, \mathbf{q}, \mathbf{n}, \mathbf{v}$  and  $z$  also apply for non-spinning compact binaries. Therefore, the explicit expressions for the quadrupolar order GW polarization states in terms of the relevant dynamical variables are again obtained by evaluating the dot products appearing in Eqs. (2.5). It is natural to invoke an inertial frame associated with  $\mathbf{L}$  to describe the orbital dynamics of non-spinning compact binaries. This is because  $\mathbf{L}$  is conserved both in magnitude and direction for non-spinning compact binaries. Furthermore, it is convenient to introduce polar coordinates  $(r, \phi)$  in a plane perpendicular to  $\mathbf{L}$  as the orbital motion takes place in such a plane. This allows us to describe  $\mathbf{r}$  and  $\mathbf{v}$  in terms of  $r, \phi$  and their time derivatives in the  $\mathbf{L}$  based inertial triad. However, it is customary to evaluate the dot products appearing in Eqs. (2.5) by expressing  $\mathbf{r}$  and  $\mathbf{v}$  in an  $\mathbf{N}$  based inertial frame  $(\mathbf{p}, \mathbf{q}, \mathbf{N})$ . This is achieved by noting that the angle  $\theta$  between  $\mathbf{N}$  and  $\mathbf{k}$ , namely the orbital inclination, remains a constant for non-spinning compact binaries. This leads to the following expressions for  $\mathbf{r}$  and  $\mathbf{v}$  in the  $(\mathbf{p}, \mathbf{q}, \mathbf{N})$  frame.

$$\mathbf{n} = -\mathbf{p} \sin \phi + (\mathbf{q} \cos \theta + \mathbf{N} \sin \theta) \cos \phi, \quad (3.1a)$$

$$\begin{aligned} \mathbf{v} = & \mathbf{p} \left( -\dot{r} \sin \phi - r \dot{\phi} \cos \phi \right) \quad (3.1b) \\ & + (\mathbf{q} \cos \theta + \mathbf{N} \sin \theta) \left( \dot{r} \cos \phi - r \dot{\phi} \sin \phi \right). \end{aligned}$$

The above expressions allow us to compute the dot products appearing in the Eqs. (2.5) for  $h_{+|Q}(l)$  and  $h_{\times|Q}(l)$ , in a straightforward manner. The resulting GW polarization states read

$$\begin{aligned} h_{+|Q} = & \frac{G\mu}{c^4 R} \times \quad (3.2a) \\ & \left\{ (1 + C_\theta^2) \left[ (z + r^2 \dot{\phi}^2 - \dot{r}^2) \cos 2\phi \right. \right. \\ & \left. \left. + 2r\dot{r}\dot{\phi} \sin 2\phi \right] - S_\theta^2 (z - r^2 \dot{\phi}^2 - \dot{r}^2) \right\}, \end{aligned}$$

$$\begin{aligned} h_{\times|Q} = & 2 \frac{G\mu}{c^4 R} C_\theta \times \quad (3.2b) \\ & \left\{ (z + r^2 \dot{\phi}^2 - \dot{r}^2) \sin 2\phi - 2r\dot{r}\dot{\phi} \cos 2\phi \right\}, \end{aligned}$$

where  $\dot{\phi} = d\phi/dt$ .

It should be obvious that we need to describe how  $r, \dot{r}, \phi$  and  $\dot{\phi}$  evolve in time for non-spinning compact binaries moving in hyperbolic orbits to obtain the associated  $h_{+|Q}(t)$  and  $h_{\times|Q}(t)$ . This is implemented in a parametric manner invoking the 1PN accurate quasi-Keplerian parameterization of Ref. [10]. The radial and angular parts of the orbital dynamics are parametrically given by

$$r = a_r (e_r \cosh v - 1), \quad (3.3a)$$

$$\phi - \phi_0 = 2K \arctan \left[ \left( \frac{e_\phi + 1}{e_\phi - 1} \right)^{1/2} \tanh v/2 \right]. \quad (3.3b)$$

The temporal evolution for  $r$  and  $\phi$  are provided numerically by tackling the 1PN accurate Kepler equation

$$l = \bar{n}(t - t_0) = e_t \sinh v - v. \quad (3.4)$$

The additional orbital parameters  $K$  and  $e_\phi$  that appear in the angular part of the parametric solution are the hyperbolic versions of the periastron advance constant and angular eccentricity associated with the eccentric orbits [10]. All the orbital elements, as expected, are PN accurate functions of conserved orbital energy and angular momentum. The 1PN accurate expressions for these orbital elements in terms of the conserved energy and angular momentum are provided by Eqs. (3.6) and (4.13) in Ref. [10]. These inputs allow us to compute 1PN accurate expressions for  $r, \dot{r}, \phi$  and  $\dot{\phi}$  in terms of  $v, e_t, \bar{n}, m$  and  $\eta$ . The explicit expressions of these dynamical variables are

$$r(v) = \frac{Gm}{c^2} \frac{1}{\bar{\xi}^{2/3}} (e_t \cosh v - 1) \left\{ 1 + \bar{\xi}^{2/3} \frac{2\eta - 18 - (6 - 7\eta)e_t \cosh v}{6(e_t \cosh v - 1)} \right\}, \quad (3.5a)$$

$$\dot{r}(v) = \bar{\xi}^{1/3} \frac{c e_t \sinh v}{e_t \cosh v - 1} \left\{ 1 - \bar{\xi}^{2/3} \frac{6 - 7\eta}{6} \right\}, \quad (3.5b)$$

$$\phi(v) - \phi_0 = 2 \arctan \left[ \left( \frac{e_\phi + 1}{e_\phi - 1} \right)^{1/2} \tanh v/2 \right] \left\{ 1 + \bar{\xi}^{2/3} \frac{3}{e_t^2 - 1} \right\}, \quad (3.5c)$$

$$\dot{\phi}(v) = \frac{\bar{n} \sqrt{e_t^2 - 1}}{(e_t \cosh v - 1)^2} \left\{ 1 - \bar{\xi}^{2/3} \frac{[3 - (4 - \eta)e_t^2 + (1 - \eta)e_t \cosh v]}{(e_t^2 - 1)(e_t \cosh v - 1)} \right\}. \quad (3.5d)$$

To obtain Eqs. (3.5), we have used PN accurate relations connecting  $e_r$  and  $e_\phi$  to  $e_t$ , namely  $e_r = e_t \{1 - \bar{\xi}^{2/3}(8 - 3\eta)/2\}$  and  $e_\phi = e_t \{1 - \bar{\xi}^{2/3}(4 - \eta)\}$ . The fact that we have invoked  $e_t$  to characterize the dynamics allows us to invoke Mikkola's approach to numerically solve the classical Kepler equation for hyperbolic orbits as detailed in Sec. 4 in Ref. [28]. We use the resulting  $v(l)$  in Eqs. (3.5) to obtain 1PN accurate  $l$  evolution for  $r, \dot{r}, \phi$  and  $\dot{\phi}$  for a non-spinning compact binary characterized by  $m, \eta, \bar{n}$  and  $e_t$ . These evolutions are implemented in Eqs. (3.2) to obtain  $h_{+|Q}(t)$  and  $h_{\times|Q}(t)$  associated with compact binaries moving in 1PN accurate hyperbolic orbits.

We move on to compute explicit expressions for  $h_+$  and

$h_\times$  that are also 1PN accurate in their amplitudes. This requires us to implement Eqs. (2.3) for  $h_+$  and  $h_\times$  while using the 1PN accurate expression for  $h_{ij}^{\text{TT}}$  for general orbits that are available in Refs. [33, 34]. The resulting 1PN accurate amplitude corrected expressions for  $h_+$  and  $h_\times$  can be written as

$$h_+ = \frac{G\mu}{c^4 R} \left( h_+^N + \frac{1}{c} h_+^{0.5} + \frac{1}{c^2} h_+^1 \right), \quad (3.6a)$$

$$h_\times = \frac{G\mu}{c^4 R} \left( h_\times^N + \frac{1}{c} h_\times^{0.5} + \frac{1}{c^2} h_\times^1 \right), \quad (3.6b)$$

where  $h_{+, \times}^N, h_{+, \times}^{0.5}$  and  $h_{+, \times}^1$  are given by

$$h_+^N = 2r\dot{r}\dot{\phi}(1 + C_\theta^2) \sin 2\phi + (1 + C_\theta^2) \left( z + r^2\dot{\phi}^2 - \dot{r}^2 \right) \cos 2\phi + S_\theta^2 \left( \dot{r}^2 + r^2\dot{\phi}^2 - z \right), \quad (3.7a)$$

$$h_\times^N = 2C_\theta \left( z + r^2\dot{\phi}^2 - \dot{r}^2 \right) \sin 2\phi - 2C_\theta 2r\dot{r}\dot{\phi} \cos 2\phi, \quad (3.7b)$$

$$h_+^{0.5PN} = \frac{S_\theta}{2} (X_1 - X_2) \left[ (3C_\theta^2 - 1) \left( \dot{r}^2 + r^2\dot{\phi}^2 - 2z \right) \dot{r} \cos \phi + (1 + C_\theta^2) \left( \dot{r}^2 - 3r^2\dot{\phi}^2 - 2z \right) \dot{r} \cos 3\phi \right. \\ \left. - \left( \dot{r}^2 + r^2\dot{\phi}^2 - z \right) (3C_\theta^2 - 1) - z(C_\theta^2 + 5) \frac{1}{2} \right] r\dot{\phi} \sin \phi + (1 + C_\theta^2) \left( 3\dot{r}^2 - r^2\dot{\phi}^2 - \frac{7}{2}z \right) r\dot{\phi} \sin 3\phi, \quad (3.7c)$$

$$h_\times^{0.5PN} = \frac{C_\theta S_\theta}{2} (X_1 - X_2) \left[ \left( 2\dot{r}^2 + 2r^2\dot{\phi}^2 - 5z \right) r\dot{\phi} \cos \phi + \left( 6\dot{r}^2 - 2r^2\dot{\phi}^2 - 7z \right) r\dot{\phi} \cos 3\phi \right. \\ \left. + 2 \left( \dot{r}^2 + r^2\dot{\phi}^2 - 2z \right) \dot{r} \sin \phi + 2 \left( \dot{r}^2 - 3r^2\dot{\phi}^2 - 2z \right) \dot{r} \sin 3\phi \right], \quad (3.7d)$$

$$\begin{aligned}
h_+^{1PN} = \frac{1}{24} & \left[ -18S_\theta^4(\dot{r}^4 + r^4\dot{\phi}^4)(3\eta - 1) + r^2\dot{\phi}^2 z S_\theta^2(51\eta - 69 + C_\theta^2 39(1 - 3\eta)) + z^2 \times \right. \\
& S_\theta^2(116 + 7(1 - 3\eta)(1 - 3C_\theta^2)) - 36\dot{r}^2 S_\theta^4 r^2 \dot{\phi}^2 (3\eta - 1) + 6r^2 z S_\theta^2(9C_\theta^2(1 - 3\eta) + 3 + 13\eta) \left. \right] \\
& + \cos 2\phi \frac{1}{2} \left[ (\dot{r}^4 - r^4\dot{\phi}^4)(1 + C_\theta^2(1 + 2S_\theta^2))(3\eta - 1) + r^2\dot{\phi}^2 z \left( (2 + 3\eta)(1 + C_\theta^2) + S_\theta^2(3\eta - 1)(4 + C_\theta^2) \right) \right. \\
& - \dot{r}^2 z \left( (3 + 2\eta)(1 + C_\theta^2) + 6C_\theta^2 S_\theta^2(3\eta - 1) \right) + z^2 \frac{1}{3} \left( 7C_\theta^2 S_\theta^2(3\eta - 1) - 29(1 + C_\theta^2) \right) \left. \right] \\
& + \cos 4\phi \frac{(1 + C_\theta^2)S_\theta^2}{24} (3\eta - 1) \left[ 6(\dot{r}^4 + r^4\dot{\phi}^4) + 51r^2\dot{\phi}^2 z + 7z^2 - 18\dot{r}^2(2r^2\dot{\phi}^2 + z) \right] \\
& - \sin 2\phi r\dot{r}\dot{\phi} \left[ (1 + C_\theta^2(1 + 2S_\theta^2))(\dot{r}^2 + r^2\dot{\phi}^2)(3\eta - 1) - z \left( (2 + 4\eta)(1 + C_\theta^2) + \frac{S_\theta^2}{2}(3\eta - 1)(1 + 9C_\theta^2) \right) \right] \\
& - \sin 4\phi r\dot{r}\dot{\phi} (3\eta - 1)(1 + C_\theta^2)S_\theta^2 \left( \dot{r}^2 - r^2\dot{\phi}^2 - \frac{9}{4}z \right), \tag{3.7e}
\end{aligned}$$

$$\begin{aligned}
h_\times^{1PN} = z r \dot{r} \dot{\phi} (1 - 3\eta) \frac{C_\theta S_\theta^2}{2} & + \cos 2\phi r \dot{r} \dot{\phi} C_\theta \left[ 2(1 + S_\theta^2)(3\eta - 1)(\dot{r}^2 + r^2\dot{\phi}^2) - z \left( 4 + 8\eta + 5S_\theta^2(3\eta - 1) \right) \right] \\
& + \cos 4\phi r \dot{r} \dot{\phi} (3\eta - 1) C_\theta S_\theta^2 \left[ 2\dot{r}^2 - 2r^2\dot{\phi}^2 - \frac{9}{2}z \right] + \sin 2\phi C_\theta \left[ (\dot{r}^4 - r^4\dot{\phi}^4)(1 + S_\theta^2)(3\eta - 1) + z \frac{r^2\dot{\phi}^2}{2} \times \right. \\
& (4 + 6\eta + 5S_\theta^2(3\eta - 1)) + z^2 \frac{1}{6}(-58 + 7S_\theta^2(3\eta - 1)) - \dot{r}^2 z (3 + 2\eta + S_\theta^2(9\eta - 3)) \left. \right] \\
& + \sin 4\phi (3\eta - 1) \frac{C_\theta S_\theta^2}{12} \left[ 6\dot{r}^4 + 6r^4\dot{\phi}^4 + 51r^2\dot{\phi}^2 z + 7z^2 - 18\dot{r}^2 \left( 2r^2\dot{\phi}^2 + z \right) \right]. \tag{3.7f}
\end{aligned}$$

We have verified that in the circular limit the above expressions reduce to Eqs. (3) and (4) in Ref. [29]. This requires us to equate  $\dot{r}$  and  $\dot{\phi}$  to zero and  $v/r$ , respectively, while replacing  $\phi$  by  $\phi + \pi/2$ . This is done to make sure that the orbital phase is measured from the same axis as in [29]. Afterwards, we need to connect  $v$  and  $z$  by the 1PN-accurate relation  $v = z^{1/2} + z^{3/2}(\eta - 3)/(2c^2)$  and express  $z$  to the variable  $x = (Gm\dot{\phi}/c^3)^{2/3}$  of Ref. [29] through the 1PN-accurate relation  $z = c^2 x (1 + (3 - \eta)x/3)$ .

We are now in a position to plot the Newtonian, 0.5PN and 1PN contributions to GW polarization states for non-spinning compact binaries moving in 1PN accurate hyperbolic orbits. This is pursued in Fig. 5 for a binary having  $m_1 = 8M_\odot, m_2 = 13M_\odot$  to compare with Figs. 6-10 in Ref. [11] while choosing  $e_t$  to be 1.3 and 2. The first three rows display the Newtonian, 0.5PN and 1PN contributions to  $h_+$  and  $h_\times$  for binaries having fully 1PN accurate orbital evolution while the amplitude contributions are fully 1PN accurate for the fourth row plots. Apart from the change in their amplitudes, there are no changes in the way various contributions temporally evolve as we vary the orbital eccentricity. To make sure of the correctness of our approach, we have reproduced temporal evolution for the real and imaginary parts of the time derivatives of mass

and current multipole moments that are displayed in Fig. 8 of [9]. Additionally, we are also able to reproduce temporal evolution for the real and imaginary parts of the (2, 2) GW mode depicted in Fig. 2 of [26] by our approach.

However, a visual comparison of our  $e_t = 2$  plots that appear in the first three rows of Fig. 5 with similar plots in Figs. 6,7 and 10 of Ref. [11] reveals substantial differences. The differences are clearly noticeable for the cross polarization states. Interestingly, plots in Figs. 8 of Ref. [11] that display what they describe as the multipolar 1PN corrections to GW polarization states are qualitatively in agreement with  $e_t = 2$  plots in the third row of our Fig. 5. The nature of the memory effect exhibited by the Newtonian contribution to  $h_\times$ , as shown in Fig. 6 of Ref. [11], is also qualitatively different from our plots and those available in the literature. We suspect that the observed differences may be due to the way temporal evolution is implemented in Ref. [11]. Note that this is implemented analytically as a PN series in terms of the coordinate time as evident from the PN accurate expression for their angular variable [11]. However, we describe orbital dynamics in a parametric way and invoke numerical solution of the PN accurate Kepler equation to obtain the time evolution. It will be interesting to probe why these approaches differ for hyperbolic orbits.

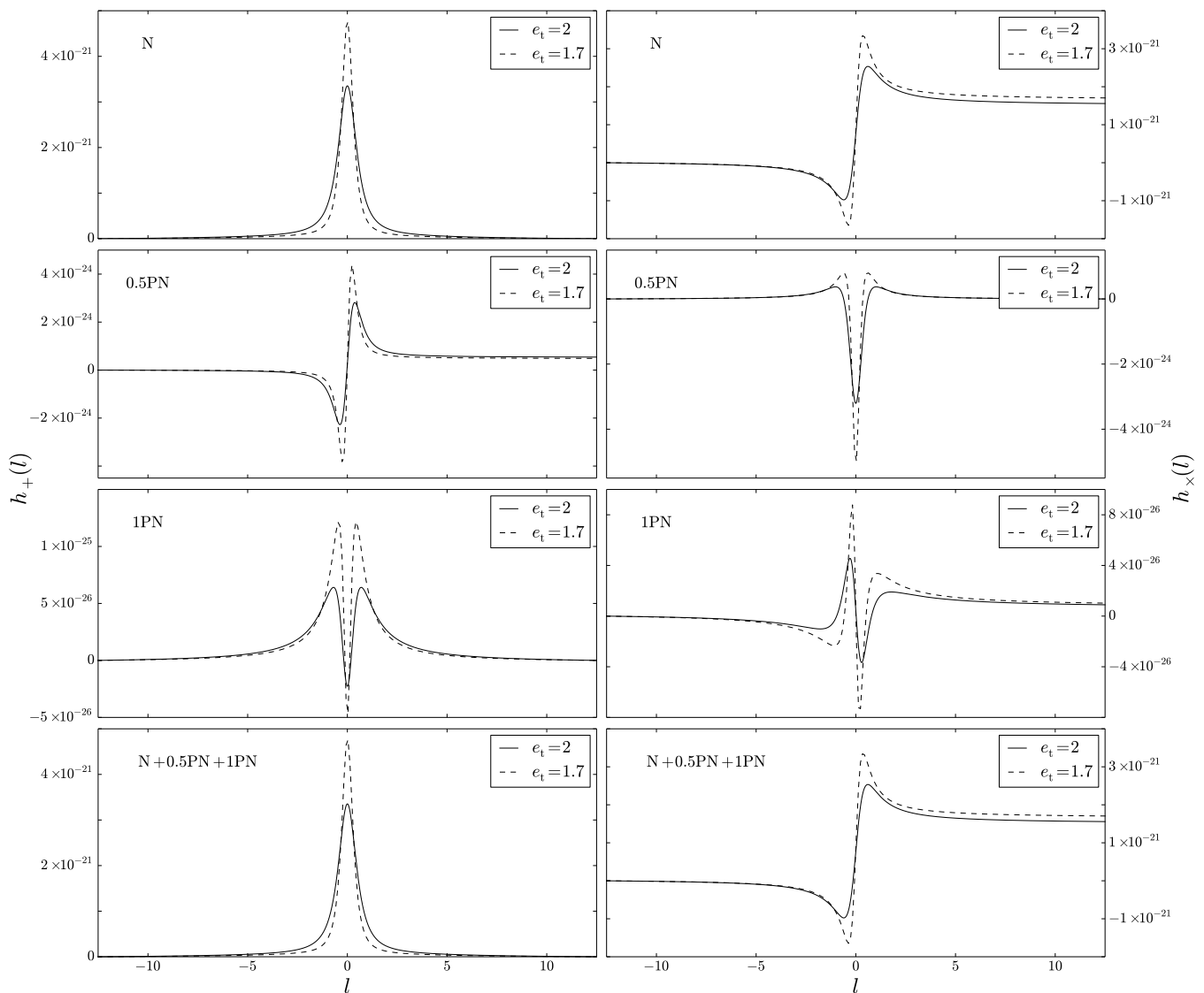


FIG. 5: Polarization states at Newtonian, 0.5PN and 1PN order, as well as their sum, respectively, as functions of  $l$  for non-spinning compact binaries in hyperbolic orbits. The solid line shows the case where  $e_t = 2$  and the dashed line shows the waveform for  $e_t = 1.7$ . The masses are  $m_1 = 8 M_\odot$  and  $m_2 = 13 M_\odot$ , while the minimal distance is chosen to be  $r_{\min} \sim 1.9 \times 10^9 m$ , as in Ref. [11]. The waveform for the  $h_+$  polarization is shown on the left and  $h_\times$  appears on the right.

We turn to explain the presence of *linear memory effect* in both the quadrupolar order polarization states of spinning compact binaries in hyperbolic orbits. We begin by explaining, in detail, why only the cross polarization state exhibits the effect in the case of non-spinning compact binaries during hyperbolic encounters with the help of Refs. [25, 26]. This diversion is desirable as we can pinpoint the terms that explicitly cause the memory effect for such binaries. Unfortunately, this is rather impossible in the case of spinning compact binaries in hyperbolic orbits as several dynamical variables, present in the Eqs. (2.1) and (2.2) for  $h_+|_Q$  and  $h_\times|_Q$ , can contribute to this effect. We begin by noting that an ideal GW detector will return to its original configuration after the passage of an incident GW, if the signal does not exhibit

any memory effect. In contrast, transient GW signals that possess memory effects force the detector not to relapse to the initial configuration even after the passage of the GW. This is essentially due to a net change in the amplitude of the local metric induced by the passage of such a GW. This leads to the linear memory effect that we observe in Fig. 5.

Influenced by Ref. [25] and with the help of Eq. (2.4), we write the net change in the quadrupolar order far-zone radiation field as

$$\Delta h_{ij}^{TT}|_Q = \frac{G}{c^4} \frac{2}{R} \Delta(\ddot{\mathcal{I}}_{ij}^{TT}), \quad (3.8)$$

where  $\mathcal{I}_{ij}$  is the mass-quadrupole moment of the binary, given by  $\mathcal{I}_{ij} = \mu x_i x_j$  at the Newtonian order. It is fairly

straightforward to compute the second time derivative of the transverse-traceless part of  $\mathcal{I}_{ij}$  using Newtonian equations of motion:  $\ddot{x}_i = -Gm x_i/r^3$ . The resulting expression reads

$$\ddot{\mathcal{I}}_{ij}^{TT} = 2\mu(\dot{x}_i \dot{x}_j - \frac{Gm}{r^3} x_i x_j) \quad (3.9)$$

The second term in Eq. (3.9) vanishes for  $t \rightarrow \pm\infty$  as it falls off like  $1/r$ . This is because  $v \rightarrow \pm\infty$  as  $t \rightarrow \pm\infty$  due to Eq. (3.4) and  $r(v)$  is proportional to  $(e_t \cosh v - 1)$  as evident from Eqs. (3.5). However, the magnitude of the relative velocity approaches a finite value, namely  $v_\infty = \sqrt{2E}$  (note that  $E$  stands for the orbital energy scaled by  $\mu$ ). This results in the following expression for the Newtonian order linear memory effect associated with hyperbolic passages

$$\Delta h_{ij} = 4 \frac{G\mu}{c^4 R} \Delta(\dot{x}_i \dot{x}_j). \quad (3.10)$$

Clearly, the differences in the components of the orbital velocity as  $t \rightarrow \pm\infty$  contribute substantially to the magnitude of memory effect.

To demonstrate explicitly the memory effect, let us consider the following scenario where the observer is perpendicular to the orbital plane ( $\theta = 0$  orientation). We infer that the non-zero components of  $\mathcal{I}_{ij}$  are  $\mathcal{I}_{11}, \mathcal{I}_{22}$  and  $\mathcal{I}_{12} = \mathcal{I}_{21}$ , where indices 1 and 2 stand for the  $x$  and  $y$  components in the  $\mathbf{j}_0$ -based inertial frame. Additionally,  $x$  and  $y$  components of the orbital velocity as  $t \rightarrow \pm\infty$  are given by

$$\lim_{t \rightarrow \pm\infty} \dot{x}_1 = \pm v_\infty \cos \pm \phi_\infty, \quad (3.11a)$$

$$\lim_{t \rightarrow \pm\infty} \dot{x}_2 = \pm v_\infty \sin \pm \phi_\infty, \quad (3.11b)$$

where  $\phi_\infty$  stands for the asymptotic value for the orbital phase as  $t \rightarrow \pm\infty$ , which can be deduced from eqs. (3.3) and (3.4). With these inputs and some trigonometric manipulations, we obtain the following expressions for the linear memory amplitudes associated with different components of  $h_{ij}$

$$\Delta h_{ii} = 0, \quad i = 1, 2, \quad (3.12a)$$

$$\Delta h_{ij} = -8 \frac{G\mu E}{c^4 R} \sin 2\phi_\infty, \quad i \neq j. \quad (3.12b)$$

In what follows we show that our expressions for the quadrupolar order  $h_+$  and  $h_\times$ , given by Eqs. (3.2), are indeed consistent with the above estimates.

To make contact with the above discussions, we consider again the binary configuration having  $\theta = 0$ . It is fairly straightforward to obtain  $t \rightarrow \pm\infty$  limits of our quadrupolar order expressions for  $h_+|_Q(t)$  and  $h_\times|_Q(t)$ , given by Eqs. (3.2). It may be recalled that  $v$  also approaches  $\pm\infty$  as  $t \rightarrow \pm\infty$  due to Eq. (3.4). This ensures that the dynamical variables  $z(v) = Gm/r(v), \dot{\phi}(v)$  and the product  $r(v)\dot{\phi}(v)$ , displayed in Eqs. (3.5), go to zero in the limit  $v \rightarrow \pm\infty$ . This is of course due to the presence of  $(e_t \cosh v - 1)$  and its powers in the denominators

of these parametric expressions. However, the expression for  $\dot{r}(v)$  does not vanish as  $t \rightarrow \pm\infty$ , but rather tends to the finite value, namely  $v_\infty$ . This forces the expressions for  $h_+|_Q(t)$  and  $h_\times|_Q(t)$ , given by Eqs. (3.2), at  $t \rightarrow +\infty$  to be

$$h_+|_Q = -2 \frac{G\mu}{c^4 R} v_\infty^2 \cos 2\phi_\infty, \quad (3.13a)$$

$$h_\times|_Q = -2 \frac{G\mu}{c^4 R} v_\infty^2 \sin 2\phi_\infty. \quad (3.13b)$$

Note that the right hand side of Eq. (3.13a) is an even function of  $\phi$  due to the presence of  $\cos 2\phi$ . However, the right hand side of Eq. (3.13b) is an odd function of  $\phi$ . This implies that

$$\lim_{t \rightarrow +\infty} h_+|_Q(t) = \lim_{t \rightarrow -\infty} h_+|_Q(t), \quad (3.14a)$$

$$\lim_{t \rightarrow +\infty} h_\times|_Q(t) = - \lim_{t \rightarrow -\infty} h_\times|_Q(t). \quad (3.14b)$$

Therefore, the amplitude differences in the above two polarization states between the early and late times during hyperbolic encounters are

$$\Delta h_+ = 0, \quad (3.15a)$$

$$\Delta h_\times = -8 \frac{G\mu E}{c^4 R} \sin 2\phi_\infty, \quad (3.15b)$$

where we used the relation  $v_\infty^2 = 2E$ . Clearly, the above two expressions are identical to Eqs. (3.12) that we derived using the detailed discussions of Ref. [25]. This also explains the linear memory effect exhibited by the first row plots in Fig. 5.

It is possible to employ similar arguments to show that 0.5PN contributions to  $h_+$ , given by Eq. (3.7c), and 1PN contributions to  $h_\times$ , given by Eq. (3.7f), should exhibit the linear memory effects during the hyperbolic encounters. This is essentially due to the presence of non-vanishing odd functions  $\dot{r}^3 \cos \phi$  and  $\dot{r}^3 \cos 3\phi$ , as well as  $\dot{r}^4 \sin 2\phi$  and  $\dot{r}^4 \sin 4\phi$  in the above expressions. Terms like  $\dot{r}^3 \sin \phi$  or  $\dot{r}^3 \sin 3\phi$  appearing in the expression for  $h_\times$  at 0.5PN order will not contribute to the memory, since both the  $\dot{r}^3$  and the  $\sin \phi$  factors are odd functions of time and yield therefore an even term. The second and third row plots in Fig. 5 clearly support the above inference. In contrast, both 0.5PN order GW polarization states, depicted in Fig. 7 in [11], show the memory effect as evident from their dashed line plots. This is also applicable to 1PN order corrections to  $h_\times$  and  $h_+$ , as displayed by the dashed line plots in Fig. 9 in [11], that arise from perturbative description of their orbital elements. Clearly, such plots are inconsistent with plots in our Fig. 5.

When we include the spin effects, it is rather difficult to obtain similar analytic estimates to demonstrate why both polarization states should exhibit the linear memory effect. However, note that the expressions for both  $h_+|_Q(t)$  and  $h_\times|_Q(t)$  contain terms like  $\dot{r}^2 \sin 2\Phi(t)$  as evident from our Eqs. (2.1) and (2.2). Additionally,

the phasing angle  $\Phi(t)$  does not have the same value at  $t = \pm\infty$  anymore due to the spin-orbit coupling induced precession of the orbital plane. These effects force the plots of  $h_{+|Q}(t)$  and  $h_{\times|Q}(t)$  to exhibit the linear memory effect as displayed in the previous section.

Finally, let us comment about the impact of orbital eccentricity on the amplitude of the memory effect. This should be easily extractable with the help of Eq. (3.15) and the fact that the angle at infinite times  $\phi_\infty$  is related to  $e_t$  through the relation  $\cos \phi_\infty = -1/e_t$ . This relation is also equivalent to  $\sin 2\phi_\infty = -2\sqrt{e_t^2 - 1}/e_t^2$ . Therefore, the memory goes to 0 when  $e_t \rightarrow 1$  and we have  $\Delta h_\times \propto 1/e_t$  for  $e_t \gg 1$ . Moreover, the amplitude of the effect peaks at eccentricity  $e_t = \sqrt{2}$  and this is consistent with our results of the present and previous sections. Let us also comment about the plausibility of observing the influences of memory effect. Unfortunately, laser interferometric GW observatories are not the ideal instruments to probe the implications of both linear and non-linear memory effects as explained in Ref. [25]. This is essentially because the internal forces present in such instruments are expected to bring the test masses back to their original (or initial) configurations. However, it may be possible to detect the implications of non-linear memory effects associated with the merger of supermassive black hole binaries with the help of the ongoing and planned pulsar timing arrays (PTAs) [35]. This is despite the fact that characteristic merger frequencies of such binaries are far higher than the nano-Hertz regime, relevant for PTAs.

#### IV. CONCLUSIONS

We provided an efficient prescription to compute GW polarizations that are PN accurate both in amplitude and phase evolution for spinning compact binaries in hyperbolic orbits. The incorporated spin effects are due to the dominant order spin-orbit interactions while the non-spinning orbital dynamics is 1PN accurate. The radial part of the conservative 1.5PN accurate orbital dynamics is treated in a parametric way by adapting the Keplerian type parametric solution for eccentric orbits, available in Ref. [31]. We invoked Mikkola's accurate and efficient method to numerically solve the hyperbolic version of the Kepler Equation to obtain temporal evolution for  $r$  and  $\dot{r}$ . In contrast, the 1.5PN accurate angular sector of the dynamics is tackled numerically by solving differential equations that describe the orbital phase evolution and the precessional dynamics of  $\mathbf{s}_1$ ,  $\mathbf{s}_2$  and  $\mathbf{k}$ . We also incorporated the influence of GW emission on this 1.5PN accurate orbital dynamics. Afterwards, we numerically inserted the variables that describe the radial, angular and precessional aspects of the orbital dynamics into PN accurate expressions for the two GW polarization states for compact binaries in general orbits. This is how we constructed ready-to-use waveforms for spinning compact binaries in hyperbolic orbits.

We observed the presence of linear GW memory effect in both the polarization states. In contrast, only the cross polarization state exhibits the memory effect for non-spinning compact binaries in hyperbolic orbits and we provided an explanation for these observations. We explored the influence of orbital eccentricity, mass ratio and dominant spin orientation on the evolution of the two polarization states and the amplitude of the memory effect. Invoking the non-spinning version of our approach, we have reproduced the temporal evolution for the real and imaginary parts of the time derivatives of mass and current multipole moments and associated GW modes, detailed in Refs. [9, 26]. However, various temporally evolving PN contributions to  $h_+$  and  $h_\times$  associated with non-spinning compact binaries, displayed in Figs. 6, 7, 9 and 10 of Ref. [11], are visually different from what we obtained. We provided a possible qualitative explanation for these differences.

It will be interesting to incorporate the 2PN order non-spinning contributions to our 1.5PN accurate orbital dynamics. This is rather tricky due to the appearance of 2PN order  $f - u \equiv 2 \tan^{-1}(\beta_\phi \sin u / (1 - \beta_\phi \cos u))$  term in the PN accurate Kepler Equation for eccentric binaries, where  $\beta_\phi = (1 - \sqrt{1 - e_\phi^2})/e_\phi$  and  $f$  is the true anomaly [36, 37]. The presence of the above  $f - u$  term leads to certain imaginary terms in the 2PN accurate Kepler Equation while adapting the usual argument of analytic continuation, namely  $u \rightarrow iv$ , to obtain its hyperbolic version. An interesting extension will be to incorporate the effects of dominant order spin-spin interactions. Another challenging direction will be to adapt Refs. [38, 39] to describe GW burst signals while employing the framework of effective-one-body formalism. It will be also desirable to pursue possible data analysis implications of these templates. A possible direction may involve probing the ability of GW search algorithms like in Ref. [40], constructed to capture unmodeled gravitational-wave bursts, to detect and distinguish our accurately modeled GW bursts.

#### Acknowledgments

We would like to thank Simone Balmelli and Cédric Huwyler for useful discussions, and the SNF for hosting AG at the Physik-Institut in Zürich during the initial stages of this work. We thank C. Berry for his detailed review of this article and the referee for many helpful suggestions. This is a LIGO document, ligo-p1400065.

### Appendix A: 1PN accurate polarization states expressions for spinning binaries

We list below the 1PN accurate expressions for  $h_+$  and  $h_\times$  for spinning binaries on general orbits in a compact form that incorporate 1PN accurate non-spinning and 1PN order spin-orbit contributions.

$$\begin{aligned}
h_+ = & 2 \frac{G\mu}{c^4 R} \left\{ \left[ \left( (\mathbf{q} \cdot \mathbf{n})^2 - (\mathbf{p} \cdot \mathbf{n})^2 \right) z + (\mathbf{p} \cdot \mathbf{v})^2 - (\mathbf{q} \cdot \mathbf{v})^2 \right] - \frac{X_1 - X_2}{2c} \left[ ((\mathbf{N} \cdot \mathbf{n}) \dot{r} - (\mathbf{N} \cdot \mathbf{v})) z (\mathbf{p} \cdot \mathbf{n})^2 \right. \right. \\
& - 6z (\mathbf{N} \cdot \mathbf{n}) (\mathbf{p} \cdot \mathbf{n}) (\mathbf{p} \cdot \mathbf{v}) + (-3 (\mathbf{N} \cdot \mathbf{n}) \dot{r} + (\mathbf{N} \cdot \mathbf{v})) z (\mathbf{q} \cdot \mathbf{n})^2 + 6z (\mathbf{N} \cdot \mathbf{n}) (\mathbf{q} \cdot \mathbf{n}) (\mathbf{q} \cdot \mathbf{v}) \\
& + 2 \left( (\mathbf{p} \cdot \mathbf{v})^2 - (\mathbf{q} \cdot \mathbf{v})^2 \right) (\mathbf{N} \cdot \mathbf{v}) \left. \right] + \frac{1}{6c^2} \left[ 6 (\mathbf{N} \cdot \mathbf{v})^2 ((\mathbf{p} \cdot \mathbf{v})^2 - (\mathbf{q} \cdot \mathbf{v})^2) (1 - 3\eta) + ([6\eta - 2] (\mathbf{N} \cdot \mathbf{v})^2 (\mathbf{p} \cdot \mathbf{n})^2 \right. \\
& + (96\eta - 32) (\mathbf{N} \cdot \mathbf{v}) (\mathbf{N} \cdot \mathbf{n}) (\mathbf{p} \cdot \mathbf{v}) (\mathbf{p} \cdot \mathbf{n}) + (-6\eta + 2) (\mathbf{N} \cdot \mathbf{v})^2 (\mathbf{q} \cdot \mathbf{n})^2 + (-96\eta + 32) (\mathbf{N} \cdot \mathbf{v}) (\mathbf{N} \cdot \mathbf{n}) \\
& \times (\mathbf{q} \cdot \mathbf{v}) (\mathbf{q} \cdot \mathbf{n}) + [(-14 + 42\eta) (\mathbf{N} \cdot \mathbf{n})^2 - 4 + 6\eta] (\mathbf{p} \cdot \mathbf{v})^2 + [(-42\eta + 14) (\mathbf{N} \cdot \mathbf{n})^2 + 4 - 6\eta] (\mathbf{q} \cdot \mathbf{v})^2 z \\
& + \left( (-9\eta + 3) (\mathbf{p} \cdot \mathbf{v})^2 + (-3 + 9\eta) (\mathbf{q} \cdot \mathbf{v})^2 \right) v^2 + ([29 + (7 - 21\eta) (\mathbf{N} \cdot \mathbf{n})^2] (\mathbf{p} \cdot \mathbf{n})^2 + [-29 + (21\eta - 7) \\
& \times (\mathbf{N} \cdot \mathbf{n})^2] (\mathbf{q} \cdot \mathbf{n})^2) z^2 + (((-9\eta + 3) (\mathbf{N} \cdot \mathbf{n})^2 - 10 - 3\eta) (\mathbf{p} \cdot \mathbf{n})^2 + ((-3 + 9\eta) (\mathbf{N} \cdot \mathbf{n})^2 + 10 + 3\eta) \\
& \times (\mathbf{q} \cdot \mathbf{n})^2) z v^2 + ((-36\eta + 12) (\mathbf{N} \cdot \mathbf{v}) (\mathbf{N} \cdot \mathbf{n}) (\mathbf{p} \cdot \mathbf{n})^2 + ((-90\eta + 30) (\mathbf{N} \cdot \mathbf{n})^2 + 20 + 12\eta) (\mathbf{p} \cdot \mathbf{v}) (\mathbf{p} \cdot \mathbf{n}) \\
& + (-12 + 36\eta) (\mathbf{N} \cdot \mathbf{v}) (\mathbf{N} \cdot \mathbf{n}) (\mathbf{q} \cdot \mathbf{n})^2 + \left. \left( (90\eta - 30) (\mathbf{N} \cdot \mathbf{n})^2 - 12\eta - 20 \right) (\mathbf{q} \cdot \mathbf{v}) (\mathbf{q} \cdot \mathbf{n}) \right] z \dot{r} \\
& + \left. \left[ [(45\eta - 15) (\mathbf{N} \cdot \mathbf{n})^2 - 9\eta + 3] (\mathbf{p} \cdot \mathbf{n})^2 + \left( (15 - 45\eta) (\mathbf{N} \cdot \mathbf{n})^2 - 3 + 9\eta \right) (\mathbf{q} \cdot \mathbf{n})^2 \right] \right\} + \frac{z^2}{c^2} \left[ (\mathbf{p} \cdot \mathbf{n}) \right. \\
& \times (X_2 \chi_2 [\mathbf{p} \cdot (\mathbf{s}_2 \times \mathbf{N})] - X_1 \chi_1 [\mathbf{p} \cdot (\mathbf{s}_1 \times \mathbf{N})]) + (\mathbf{q} \cdot \mathbf{n}) (X_1 \chi_1 [\mathbf{q} \cdot (\mathbf{s}_1 \times \mathbf{N})] - X_2 \chi_2 [\mathbf{q} \cdot (\mathbf{s}_2 \times \mathbf{N})]) \left. \right] \left. \right\}, \quad (\text{A1a})
\end{aligned}$$

$$\begin{aligned}
h_\times = & 4 \frac{G\mu}{c^4 R} \left\{ \left[ -(\mathbf{p} \cdot \mathbf{n}) (\mathbf{q} \cdot \mathbf{n}) z + (\mathbf{p} \cdot \mathbf{v}) (\mathbf{q} \cdot \mathbf{v}) \right] - \frac{X_1 - X_2}{c} \left[ \left( \{ [3 (\mathbf{N} \cdot \mathbf{n}) \dot{r} - (\mathbf{N} \cdot \mathbf{v})] (\mathbf{q} \cdot \mathbf{n}) - 3 (\mathbf{N} \cdot \mathbf{n}) (\mathbf{q} \cdot \mathbf{v}) \} \right. \right. \\
& \times (\mathbf{p} \cdot \mathbf{n}) - 3 (\mathbf{N} \cdot \mathbf{n}) (\mathbf{q} \cdot \mathbf{n}) (\mathbf{p} \cdot \mathbf{v}) \left. \right) z + 2 (\mathbf{p} \cdot \mathbf{v}) (\mathbf{q} \cdot \mathbf{v}) (\mathbf{N} \cdot \mathbf{v}) \left. \right] + \frac{1}{6c^2} \left[ 6 (1 - 3\eta) (\mathbf{N} \cdot \mathbf{v})^2 (\mathbf{p} \cdot \mathbf{v}) (\mathbf{q} \cdot \mathbf{v}) \right. \\
& + ([6\eta - 2] (\mathbf{N} \cdot \mathbf{v})^2 (\mathbf{q} \cdot \mathbf{n}) + (48\eta - 16) (\mathbf{N} \cdot \mathbf{v}) (\mathbf{N} \cdot \mathbf{n}) (\mathbf{q} \cdot \mathbf{v})] (\mathbf{p} \cdot \mathbf{n}) + (48\eta - 16) (\mathbf{N} \cdot \mathbf{v}) (\mathbf{N} \cdot \mathbf{n}) (\mathbf{p} \cdot \mathbf{v}) (\mathbf{q} \cdot \mathbf{n}) \\
& + \left( (-14 + 42\eta) (\mathbf{N} \cdot \mathbf{n})^2 - 4 + 6\eta \right) (\mathbf{q} \cdot \mathbf{v}) (\mathbf{p} \cdot \mathbf{v}) z + (-9\eta + 3) (\mathbf{q} \cdot \mathbf{v}) (\mathbf{p} \cdot \mathbf{v}) v^2 + (29 + (7 - 21\eta) (\mathbf{N} \cdot \mathbf{n})^2) \\
& \times (\mathbf{q} \cdot \mathbf{n}) (\mathbf{p} \cdot \mathbf{n}) z^2 + ((-9\eta + 3) (\mathbf{N} \cdot \mathbf{n})^2 - 10 - 3\eta) (\mathbf{q} \cdot \mathbf{n}) (\mathbf{p} \cdot \mathbf{n}) z v^2 + ((-36\eta + 12) (\mathbf{N} \cdot \mathbf{v}) (\mathbf{N} \cdot \mathbf{n}) (\mathbf{q} \cdot \mathbf{n}) \\
& + \left( (15 - 45\eta) (\mathbf{N} \cdot \mathbf{n})^2 + 10 + 6\eta \right) (\mathbf{q} \cdot \mathbf{v}) (\mathbf{p} \cdot \mathbf{n}) + [(15 - 45\eta) (\mathbf{N} \cdot \mathbf{n})^2 + 10 + 6\eta] (\mathbf{p} \cdot \mathbf{v}) (\mathbf{q} \cdot \mathbf{n}) \dot{r} z + ((45\eta - 15) \\
& \times (\mathbf{N} \cdot \mathbf{n})^2 - 9\eta + 3) (\mathbf{q} \cdot \mathbf{n}) (\mathbf{p} \cdot \mathbf{n}) \dot{r}^2 z \left. \right] + \frac{z^2}{c^2} (\mathbf{q} \cdot \mathbf{n}) \left[ X_2 \chi_2 (\mathbf{p} \cdot (\mathbf{s}_2 \times \mathbf{N})) - X_1 \chi_1 (\mathbf{p} \cdot (\mathbf{s}_1 \times \mathbf{N})) \right] \left. \right\}. \quad (\text{A1b})
\end{aligned}$$

The dot products that appear in the above equations, as expected, are evaluated in the  $(\mathbf{p}, \mathbf{q}, \mathbf{N})$  frame. These dot products can be written in terms of the Eulerian angles  $\Phi(t)$ ,  $\alpha(t)$ ,  $\iota(t)$ , and the constant angle  $\theta$  and are given by

$$\mathbf{p} \cdot \mathbf{n} = -\cos \Phi \sin \alpha - \sin \Phi \cos \alpha \cos \iota, \quad (\text{A2})$$

$$\mathbf{q} \cdot \mathbf{n} = C_\theta (\cos \Phi \cos \alpha - \sin \Phi \sin \alpha \cos \iota) - S_\theta \sin \iota \sin \Phi, \quad (\text{A3})$$

$$\mathbf{p} \cdot \mathbf{v} = r \dot{\Phi} (\sin \Phi \sin \alpha - \cos \Phi \cos \alpha \cos \iota) - \dot{r} (\cos \Phi \sin \alpha + \sin \Phi \cos \alpha \cos \iota), \quad (\text{A4})$$

$$\mathbf{q} \cdot \mathbf{v} = \dot{r} (C_\theta (\cos \Phi \cos \alpha - \sin \Phi \sin \alpha \cos \iota) - S_\theta \sin \Phi \sin \iota) \quad (\text{A5})$$

$$- r \dot{\Phi} (C_\theta (\sin \Phi \cos \alpha + \cos \Phi \sin \alpha \cos \iota) + S_\theta \cos \Phi \sin \iota),$$

$$\mathbf{N} \cdot \mathbf{n} = C_\theta \sin \Phi \sin \iota + S_\theta (\cos \Phi \cos \alpha - \sin \Phi \sin \alpha \cos \iota), \quad (\text{A6})$$

$$\mathbf{N} \cdot \mathbf{v} = \dot{r} (S_\theta (\cos \Phi \cos \alpha - \sin \Phi \sin \alpha \cos \iota) + C_\theta \sin \Phi \sin \iota) \quad (\text{A7})$$

$$- r \dot{\Phi} (S_\theta (\sin \Phi \cos \alpha + \cos \Phi \sin \alpha \cos \iota) - C_\theta \sin \Phi \sin \iota).$$

The explicit evaluation of Eqs. (A1) with the help of the above dot products leads to amplitude corrected GW polarization states for spinning compact binaries on general orbits. We can numerically impose the evolution of various variables for the hyperbolic orbits to obtain the amplitude corrected polarization states for spinning binaries on hyperbolic orbits.

- 
- [1] The following websites provide detailed and updated informations about the ground- and space-based gravitational wave interferometers: <http://www.elisascience.org>, <http://www.virgo.ifn.it>, and <http://www.ligo.caltech.edu>.
- [2] B. Kocsis, M. E. Gáspár, and S. Márka, *Astrophys. J.* **648**, 411 (2006), [astro-ph/0603441](https://arxiv.org/abs/astro-ph/0603441).
- [3] R. O. Hansen, *Phys. Rev. D* **5**, 1021 (1972).
- [4] M. Walker and C. M. Will, *Phys. Rev. D* **19**, 3483 (1979).
- [5] G. M. Harry and the LIGO Scientific Collaboration, *Classical and Quantum Gravity* **27**, 084006 (2010).
- [6] R. M. O’Leary, B. Kocsis, and A. Loeb, *Mon. Not. R. Astr. Soc.* **395**, 2127 (2009), 0807.2638.
- [7] D. Tsang, *Astrophys. J.* **777**, 103 (2013), 1307.3554.
- [8] M. Turner, *Astrophys. J.* **216**, 914 (1977).
- [9] W. Junker and G. Schaefer, *Mon. Not. R. Astr. Soc.* **254**, 146 (1992).
- [10] T. Damour and N. Deruelle, *Ann. Inst. Henri Poincaré Phys. Théor.*, Vol. 43, No. 1, p. 107 - 132 **43**, 107 (1985).
- [11] J. Majár, P. Forgács, and M. Vasúth, *Phys. Rev. D* **82**, 064041 (2010), [arXiv:gr-qc/1009.5042](https://arxiv.org/abs/gr-qc/1009.5042).
- [12] J. Majár and M. Vasúth, *Phys. Rev. D* **77**, 104005 (2008), 0806.2273.
- [13] R. V. Wagoner and C. M. Will, *Astrophys. J.* **210**, 764 (1976).
- [14] L. Blanchet and G. Schaefer, *Mon. Not. R. Astr. Soc.* **239**, 845 (1989).
- [15] S. J. Kovacs and K. S. Thorne, *Astrophys. J.* **217**, 252 (1977).
- [16] L. De Vittori, P. Jetzer, and A. Klein, *Phys. Rev. D* **86**, 044017 (2012), 1207.5359.
- [17] C. P. L. Berry and J. R. Gair, *Phys. Rev. D* **82**, 107501 (2010), 1010.3865.
- [18] S. Capozziello, M. de Laurentis, F. de Paolis, G. Ingrosso, and A. Nucita, *Modern Physics Letters A* **23**, 99 (2008), 0801.0122.
- [19] L. J. Rubbo, K. Holley-Bockelmann, and L. S. Finn, *The Astrophysical Journal Letters* **649**, L25 (2006).
- [20] C. P. L. Berry and J. R. Gair, *Mon. Not. R. Astr. Soc.* **429**, 589 (2013).
- [21] C. P. L. Berry and J. R. Gair, *Mon. Not. R. Astr. Soc.* **433**, 3572 (2013).
- [22] C. P. L. Berry and J. R. Gair, *Mon. Not. R. Astr. Soc.* **435**, 3521 (2013).
- [23] B. M. Barker and R. F. O’Connell, *Phys. Rev. D* **12**, 329 (1975).
- [24] L. E. Kidder, *Phys. Rev. D* **52**, 821 (1995), [gr-qc/9506022](https://arxiv.org/abs/gr-qc/9506022).
- [25] M. Favata, *Phys. Rev. D* **80**, 024002 (2009).
- [26] M. Favata, *Phys. Rev. D* **84**, 124013 (2011).
- [27] V. B. Braginskii and L. P. Grishchuk, *Zhurnal Eksperimentalnoi i Teoreticheskoi Fiziki* **89**, 744 (1985).
- [28] S. Mikkola, *Celestial Mechanics* **40**, 329 (1987).
- [29] L. Blanchet, B. R. Iyer, C. M. Will, and A. G. Wiseman, *Classical and Quantum Gravity* **13**, 575 (1996), [gr-qc/9602024](https://arxiv.org/abs/gr-qc/9602024).
- [30] T. Damour and G. Schafer, *Nuovo Cimento B Serie* **101**, 127 (1988).
- [31] A. Gopakumar and G. Schäfer, *Phys. Rev. D* **84**, 124007 (2011).
- [32] T. Damour, A. Gopakumar, and B. R. Iyer, *Phys. Rev. D* **70**, 064028 (2004), [arXiv:gr-qc/0404128](https://arxiv.org/abs/gr-qc/0404128).
- [33] C. M. Will and A. G. Wiseman, *Phys. Rev. D* **54**, 4813 (1996), [gr-qc/9608012](https://arxiv.org/abs/gr-qc/9608012).
- [34] A. Gopakumar and B. R. Iyer, *Phys. Rev. D* **56**, 7708 (1997), [gr-qc/9710075](https://arxiv.org/abs/gr-qc/9710075).
- [35] N. Seto, *Mon. Not. R. Astr. Soc.* **400**, L38 (2009).
- [36] G. Schäfer and N. Wex, *Physics Letters A* **174**, 196 (1993).
- [37] N. Wex, *Classical and Quantum Gravity* **12**, 983 (1995).
- [38] D. Bini and T. Damour, *Phys. Rev. D* **86**, 124012 (2012), 1210.2834.
- [39] T. Damour, F. Guercilena, I. Hinder, S. Hopper, A. Nagar, and L. Rezzolla, *ArXiv e-prints* (2014), 1402.7307.
- [40] E. Thrane and M. Coughlin, *Phys. Rev. D* **89**, 063012 (2014).